

# Adaptive dynamic programming-based adaptive-gain sliding mode tracking control for fixed-wing UAV with disturbances

Chaofan Zhang<sup>a</sup>, Guoshan Zhang<sup>a,\*</sup> and Qi Dong<sup>b</sup>

<sup>a</sup>*School of Electrical and Information Engineering, Tianjin University, Tianjin 300072, China*

<sup>b</sup>*China Academy of Electronics and Information Technology, Beijing 100041, China*

## ARTICLE INFO

### Keywords:

Fixed-wing UAV  
Tracking control  
Adaptive dynamic programming (ADP)  
Adaptive-gain sliding mode  
Disturbances

## ABSTRACT

This paper proposes an adaptive dynamic programming-based adaptive-gain sliding mode control (ADP-ASMC) scheme for a fixed-wing unmanned aerial vehicle (UAV) with matched and unmatched disturbances. Starting from the dynamic of fixed-wing UAV, the control-oriented model composed of attitude subsystem and airspeed subsystem is established. According to the different issues in two subsystems, two novel adaptive-gain generalized super-twisting (AGST) algorithms are developed to eliminate the effects of disturbances in two subsystems and make the system trajectories tend to the designed integral sliding manifolds (ISMs) in finite time. Then, based on the expected equivalent sliding-mode dynamics, the modified adaptive dynamic programming (ADP) approach with actor-critic (AC) structure is utilized to generate the nearly optimal control laws and achieve the nearly optimal performance of the sliding-mode dynamics. Furthermore, through the Lyapunov stability theorem, the tracking errors and the weight estimation errors of two neural networks (NNs) are all uniformly ultimately bounded (UUB). Finally, comparative simulations demonstrate the superior performance of the proposed control scheme for the fixed-wing UAV.

## 1. Introduction

During the past decades, fixed-wing unmanned aerial vehicles (UAVs) are widely employed in military and civilian aspects, such as fire detection, disaster relief, and infrastructure inspection [1]. Compared with the rotating wing vehicles, fixed-wing UAVs have some important advantages, namely, wide flight coverage and fast flight velocity [2]. However, the system of fixed-wing UAV also possesses some characteristics of high nonlinearity, stringent constraints, and strong coupling, which makes the flight control extremely difficult [3]. Beyond that, the external disturbances during the flight process will threaten the flight stability and safety of fixed-wing UAVs. Thus, it is a challenging task to design strongly robust, highly autonomous, and reliable flight control schemes for fixed-wing UAVs.

Recently, various control algorithms, for examples, model prediction control [4], dynamic surface control [5], deep reinforcement learning method [6], and linear quadratic regulator [7], have been employed in flight control field and promoted further study in this field. In addition, sliding mode control (SMC) plays an important role on designing control scheme for many complex uncertain flight systems, such as multiple UAVs [8, 9], hypersonic vehicles [10, 11], and quadrotor aircraft [12]. This algorithm ensures finite-time convergence of the sliding mode output by utilizing a discontinuous control and owns inherent insensitivity and robustness to plant uncertainties and external disturbances [13]. In addition, the SMC algorithms are combined with fuzzy logic [14], backstepping [15], and adaptive control [16, 17], to improve control performance. Although the SMC has strong robustness, it is generally designed according to the worst case. The robustness of SMC is achieved at the cost of a

high frequency switching of the control signal, which has a negative effect in the actuators [18]. Moreover, from the engineering viewpoint, it is a hard task to obtain the exact information of the bounds of disturbances/uncertainties. In such a situation, the larger control gains have to be set to ensure the system stability, which may lead to the overestimation of control gains and then easily cause the high frequency oscillations known as “chattering”, saturation, and higher energy consumption [19]. The above problem motivates the development of adaptive-gain SMC algorithms. In the context of ensuring stability, adaptive-gain SMC algorithms aim at obtaining the control gains to be as small as possible [20, 21, 22, 23, 24, 25, 26]. The adaptive-gain SMC algorithms can alleviate the undesired chattering effect and enhance the control performance effectively. In the field of flight control, different gain-adaptation laws in combination with SMC algorithms are widely utilized to design flight control scheme [27, 28, 29, 30, 31]. In the above-mentioned literatures, the gain-adaptation laws, to some extent, are able to alleviate the chattering phenomenon of SMC for systems with unknown bounded disturbances, but there also exist a few problems.

- For the approaches based on the utilization of equivalent control, the adaptive-gains in second layer are monotonically increasing and will be fixed at a constant once the states reach the predefined domain [23]. The overestimation may not be avoided in the second-layer gains if dealing with the time-varying disturbances, which further affects the values of the first-layer control gains.
- For the approaches based on increasing and decreasing the gains, the gains increase until the sliding mode is achieved and then decrease until the moment it is

\*Corresponding author: Guoshan Zhang (zhanggs@tju.edu.cn)  
ORCID(s):

lost. By using this approach, the sliding variables can only converge to the neighborhood of origin, which means that the sliding mode cannot be reached any more [25, 32].

- For some existing adaptive-gain SMC algorithms, the two control gains are tuned by the same gain-adaptation laws [21, 22, 27, 28]. The parameter selection of this design is simple, but there exists a shortcoming that the control performance may be influenced when handling the state- and time-dependent disturbances simultaneously.

Under the premise of robustness and stability, the optimality is another important performance index. The objective of optimal control is to stabilize the system and meanwhile optimize a predefined cost function composed of states and control inputs [33]. During the past several years, many researchers have paid attentions to employing adaptive dynamic programming (ADP) approaches to address optimal control problems [34, 35]. Referring to [36, 37, 38, 39], ADP approaches have been applied to many fields, for example, power system, single link robot arm system, flight control system and so on. However, it is difficult to implement the ADP approach for the nonlinear systems with time-varying disturbances. In order to solve this problem, the control scheme combining integral sliding-mode control (ISMC) algorithm with ADP approach is presented [40, 41, 42, 43], where ADP approach is used to obtain the nearly optimal control laws for the sliding-mode dynamics.

Motivated by the above mentioned research, an adaptive dynamic programming-based adaptive-gain sliding mode control (ADP-ASMC) scheme is constructed for fixed-wing UAVs with unknown unmatched/matched disturbances. The main contributions of our work are summarized as follows.

1. A flight control scheme constructed with SMC algorithms and ADP approach is developed for fixed-wing UAV for the first time. The proposed control scheme not only handles the effects of unknown disturbances but also optimizes the performance index when the system trajectory move on the ISMs. To some extent, the robustness and optimality are both guaranteed.
2. According to the different characteristics of attitude and airspeed subsystem, two novel adaptive-gain generalized super-twisting (AGST) algorithms with modified gain-adaptation laws are developed to handle the unknown bounded disturbances. In the designed algorithms, the prior knowledge of disturbances is not required and chattering phenomenon can be attenuated efficiently.
3. A modified ADP approach with AC structure is proposed to achieve stable and provide nearly optimal control performance of the sliding mode dynamics. The nonlinear tracking problem can be solved effectively through segmenting an error term from the optimal performance index, and no initial stabilizing control inputs are required in the training process.

The remainder of this paper is organized as follows. The dynamic model of fixed-wing UAV and the control-oriented models (COMs) of two subsystems are given in Section 2. In Section 3, the proposed ADP-ASMC scheme is developed. The comparative simulations and conclusion are shown in Section 4 and Section 5, respectively.

## 2. Problem formulation

### 2.1. Fixed-wing UAV model

The fixed-wing UAV modelled on basis of the Newton–Euler formulation is given as [30]

$$\dot{\boldsymbol{p}}_n = \boldsymbol{R}_I \boldsymbol{v}, \quad (1)$$

$$\dot{\boldsymbol{v}} = (\boldsymbol{F} + \boldsymbol{T}) / m + \boldsymbol{R}_I \boldsymbol{g} - \boldsymbol{\omega} \times \boldsymbol{v}, \quad (2)$$

$$\dot{\boldsymbol{\Theta}} = \boldsymbol{R}_\Theta \boldsymbol{\omega}, \quad (3)$$

$$\boldsymbol{I} \dot{\boldsymbol{\omega}} = -\boldsymbol{\omega} \times \boldsymbol{I} \boldsymbol{\omega} + \boldsymbol{M}, \quad (4)$$

where  $\boldsymbol{p}_n = [p_x, p_y, p_z]^T$  denotes the positions of the UAV corresponding to  $x_i, y_i$ , and  $z_i$  (shown in Fig. 1),  $\boldsymbol{v} = [u, v, w]^T$  is the linear velocity vector,  $\boldsymbol{\Theta} = [\phi, \theta, \psi]^T$  denotes the attitude angle vector,  $\phi, \theta, \psi$  respectively denote roll angle, pitch angle, and yaw angle,  $\boldsymbol{\omega} = [p, q, r]^T$  stands for the angular rate vector composed of roll, pitch, and yaw angular rates,  $\boldsymbol{T} = [T_x, 0, 0]^T$  represents the thrust along the body axis  $x_b$ ,  $\boldsymbol{g} = [0, 0, g_z]^T$  denotes the gravity acceleration along the inertial axis  $z_i$ ,  $\boldsymbol{F} = [F_x, F_y, F_z]^T$  is the aerodynamics force vector,  $\boldsymbol{M} = [M_x, M_y, M_z]^T$  is control moment vector,  $M_x, M_y, M_z$  denote roll, pitch and yaw moment. The nominal inertia matrix  $\boldsymbol{I} \in \mathbb{R}^{3 \times 3}$ , matrices  $\boldsymbol{R}_\Theta \in \mathbb{R}^{3 \times 3}$  and  $\boldsymbol{R}_I \in \mathbb{R}^{3 \times 3}$  are given as

$$\boldsymbol{I} = \begin{bmatrix} I_{xx} & 0 & I_{xz} \\ 0 & I_{yy} & 0 \\ I_{xz} & 0 & I_{zz} \end{bmatrix},$$

$$\boldsymbol{R}_\Theta = \begin{bmatrix} 0 & \cos \phi & -\sin \phi \\ 0 & \frac{\sin \phi}{\cos \theta} & \frac{\cos \phi}{\cos \theta} \\ 1 & \sin \phi \tan \theta & \cos \phi \tan \theta \end{bmatrix},$$

$$\boldsymbol{R}_I = \begin{bmatrix} \cos \theta \cos \psi & R_{I1} & R_{I2} \\ \cos \theta \sin \psi & R_{I3} & R_{I4} \\ -\sin \theta & \cos \theta \sin \phi & \cos \theta \cos \phi \end{bmatrix},$$

where

$$R_{I1} = \sin \theta \cos \psi \sin \phi - \sin \psi \cos \phi,$$

$$R_{I2} = \sin \theta \cdot \cos \psi \cos \phi + \sin \psi \sin \phi,$$

$$R_{I3} = \sin \theta \sin \psi \sin \phi + \cos \psi \cos \phi,$$

$$R_{I4} = \sin \theta \sin \psi \cos \phi - \cos \psi \sin \phi.$$

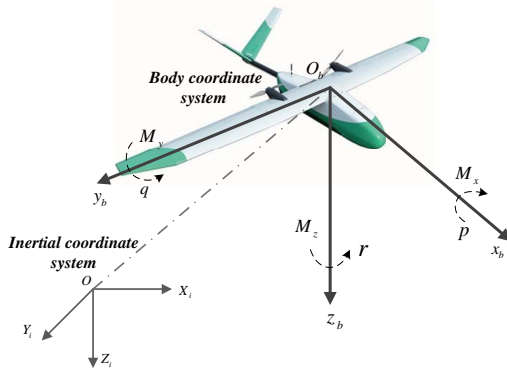


Figure 1: Referential frames configuration.

## 2.2. Control-oriented model

The control-oriented models (COMs) of fixed-wing UAV are established in this subsection. The attitude controller is designed according to the attitude subsystem (3) and (4). In our work, the attitude angle  $\Theta$  and angular rate  $\omega$  are both measurable. Considering the influence of unknown matched disturbances  $\Delta \mathbf{d}_m(t)$  and unmatched disturbances  $\Delta \mathbf{d}_u(t)$ , (3) and (4) are rewritten as

$$\begin{aligned} \dot{\Theta} &= \mathbf{R}_\Theta \omega + \Delta \mathbf{d}_u(t) \\ \dot{\omega} &= -\mathbf{I}^{-1} \omega \times \mathbf{I} \omega + \mathbf{I}^{-1} (\mathbf{M} + \Delta \mathbf{d}_m(t)). \end{aligned} \quad (5)$$

To ease the notation, we denote  $\Delta \mathbf{d}_u(t) = \Delta \mathbf{d}_u$  and  $\Delta \mathbf{d}_m(t) = \Delta \mathbf{d}_m$  in the sequel. The reference attitude command  $\Theta_d \in \mathbb{R}^{3 \times 1}$  and its derivative  $\dot{\Theta}_d$  are smooth, bounded, and known. Define that the attitude tracking error is  $e_\Theta = \Theta - \Theta_d = [e_\phi, e_\theta, e_\psi]^T$  and the dynamic of  $e_\Theta$  is

$$\dot{e}_\Theta = \mathbf{R}_\Theta \omega - \dot{\Theta}_d + \Delta \mathbf{d}_u.$$

Let  $\dot{e}_\Theta = \mathbf{z}_\Theta$  and we can obtain

$$\begin{aligned} \dot{e}_\Theta &= \mathbf{z}_\Theta \\ \dot{\mathbf{z}}_\Theta &= \mathbf{G}(\mathbf{z}_\Theta) + \mathbf{R}_\Theta \mathbf{I}^{-1} \mathbf{M} - \ddot{\Theta}_d + \Delta \mathbf{a} + \Delta \dot{\mathbf{d}}_u \end{aligned} \quad (6)$$

where  $\mathbf{G}(\mathbf{z}_\Theta) = \dot{\mathbf{R}}_\Theta \omega - \mathbf{R}_\Theta \mathbf{I}^{-1} \omega \times \mathbf{I} \omega$  and  $\Delta \mathbf{a} = \mathbf{R}_\Theta \mathbf{I}^{-1} \Delta \mathbf{d}_m$  is the lumped disturbance vector related to the states. (6) is the COM of attitude subsystem, which is a second-order multiple-input multiple-output (MIMO) system.

**Remark 1.** The pitch angle  $\theta$  cannot be equal to  $\pm \frac{\pi}{2}$  such that the matrix  $\mathbf{R}_\Theta$  is always invertible and the control moment vector  $\mathbf{M}$  is nonsingular.

**Assumption 1.** Assume that the matched disturbance  $\Delta \mathbf{d}_m$  is bounded by an unknown positive constant  $\delta_{dm}$ , i.e.,  $\|\Delta \mathbf{d}_m\| \leq \delta_{dm}$ . The unmatched disturbance  $\Delta \mathbf{d}_u$  is bounded by an unknown positive constant  $\delta_{u0}$ , namely,  $\|\Delta \mathbf{d}_u\| \leq \delta_{u0}$ . Beyond that,  $\Delta \mathbf{d}_u$  is also bounded by unknown Lipschitz constants  $\delta_{du1}$  and  $\delta_{du2}$ , namely,  $\|\Delta \dot{\mathbf{d}}_u\| \leq \delta_{du1}$  and  $\|\Delta \ddot{\mathbf{d}}_u\| \leq \delta_{du2}$ .

In fixed-wing UAV, the linear velocity vector  $\mathbf{v}$  in (2) is controlled through the airspeed controller which is designed according to the airspeed subsystem [30, 44]. Following (2), the dynamic of airspeed subsystem is derived as

$$\dot{V} = \frac{T_x \cos \alpha \cos \beta - D}{m} - g_v + \Delta_V(t), \quad (7)$$

where  $V$  denotes airspeed,  $\alpha = \arctan\left(\frac{w}{u}\right)$  and  $\beta = \arcsin\left(\frac{v}{u}\right)$  respectively represent angle of attack and sideslip angle,  $D$  represents drag,  $\Delta_V$  is external disturbance of airspeed subsystem,  $g_v$  is the term that is relevant to attitude subsystem and is given as

$$\begin{aligned} g_v &= g(-\cos \alpha \cos \beta \sin \theta + \sin \beta \sin \phi \cos \theta \\ &\quad + \sin \alpha \cos \beta \cos \phi \cos \theta). \end{aligned}$$

**Assumption 2.** The external disturbance  $\Delta_V$  is unknown but bounded, i.e.,  $|\Delta_V| \leq \delta_V$ . Besides, the derivative  $\dot{\Delta}_V$  and second derivative  $\ddot{\Delta}_V$  are also bounded, i.e.,  $|\dot{\Delta}_V| \leq \delta_{V0}$  and  $|\ddot{\Delta}_V| \leq \delta_{V1}$ .  $\delta_V$ ,  $\delta_{V0}$ , and  $\delta_{V1}$  are unknown positive constants.

$V_d$  is the reference airspeed command and the airspeed tracking error is  $e_V = V - V_d$ . The dynamic of  $e_V$  is

$$\dot{e}_V = \frac{T_x \cos \alpha \cos \beta - D}{m} - g_v - \dot{V}_d + \Delta_V(t), \quad (8)$$

which is a first-order single-input single-output (SISO) system. It should be noted that  $\alpha$  and  $\beta$  cannot be equal to  $\pm \frac{\pi}{2}$  to avoid the singularity of  $T_x$ .

Following the above analysis, (6) and (8) are the COMs utilized to design control scheme.

**Control Objective:** The aim of our work is to design the control laws  $\mathbf{M}$  and  $T_x$  for fixed-wing UAV such that the attitude angle  $\Theta$  and airspeed  $V$  can track the reference command  $\Theta_d$  and  $V_d$  under the effects of  $\Delta \mathbf{d}_u$ ,  $\Delta \mathbf{d}_m$ , and  $\Delta_V$ .

## 2.3. Preliminaries

Before the detailed control scheme design, Definition 1, Notation 1, and Proposition 1 are presented in this subsection.

**Definition 1.** [42] The equilibrium point  $\bar{x}_0$  for system

$$\dot{x}(t) = f(x(t)), x(0) = x_0 \quad (9)$$

is said to be uniformly ultimately bounded (UUB) if there exists a compact set  $\Omega \subset \mathbb{R}^n$  so that for all  $\bar{x}_0 \in \Omega$  there exists a bound  $B$  and a time  $T(B, \bar{x}_0)$  such that  $\|x(t) - \bar{x}_0\| \leq B$  for all  $t \geq t_0 + T$ .

**Notation 1.**  $\mathbb{R}$ ,  $\mathbb{R}^n$ , and  $\mathbb{R}^{m \times n}$  denote the set of real numbers, the Euclidean space of real  $n$ -vectors, and the space of  $m \times n$  real matrices, respectively. For a given state vector  $\mathbf{x} = [x_1, x_2, \dots, x_n]^T$ , define the multivariable sign function  $\mathbf{sign}(\mathbf{x}) = \frac{\mathbf{x}}{\|\mathbf{x}\|}$  and  $\|\mathbf{sign}(\mathbf{x})\| = 1$ .  $[\mathbf{x}]^\rho = \|\mathbf{x}\|^\rho \mathbf{sign}(\mathbf{x})$ .  $\|\mathbf{x}\| = \sqrt{\mathbf{x}^T \mathbf{x}}$  denotes the Euclidean norm of vectors.  $[\mathbf{x}]^\rho$

is continuous for any  $\rho > 0$  at zero and its value is understood in the sense of Filippov [45]. For a given state  $x$ ,  $[x]^\rho = |x|^\rho \text{sign}(x)$ , where  $|\cdot|$  represents the absolute value of a scalar variable and  $\text{sign}(\cdot)$  is the symbolic function. For a given matrix  $\mathbf{A}$ , define that  $\lambda_{\min}(\mathbf{A})$  and  $\lambda_{\max}(\mathbf{A})$  are the minimum and maximum eigenvalues of  $\mathbf{A}$ .  $\otimes$  represents the Kronecker product between two matrices.

**Proposition 1.** For a symmetric positive definite matrix  $\mathbf{A} \in \mathbb{R}^{m \times m}$  and  $n$ -dimension identity matrix  $\mathbf{I}_n$ , the matrix  $\tilde{\mathbf{A}} = \mathbf{A} \otimes \mathbf{I}_n \in \mathbb{R}^{mn \times mn}$  is also a symmetric positive definite matrix.

### 3. Main Results

In this section, the detailed design process of the proposed ADP-ASMC scheme is introduced.

#### 3.1. Sliding mode control design

For attitude subsystem (5) and airspeed subsystem (7), there exist the unknown disturbance  $\Delta \mathbf{d}_m$ ,  $\Delta \mathbf{d}_u$ , and  $\Delta \mathbf{v}$ , which are relevant to time  $t$ . It is difficult for the existing ADP approaches to solve the time-varying optimal control problem directly [40]. Thus, according to the different issues in two subsystems, two novel adaptive-gain generalized super-twisting (AGST) algorithms are combined with integral sliding manifolds (ISMs) to eliminate the effects of  $\Delta \mathbf{d}_m$ ,  $\Delta \mathbf{d}_u$ , and  $\Delta \mathbf{v}$ . Then, a modified ADP approach is developed in Subsection 3.2 to generate the nearly optimal control laws for the sliding mode dynamics. In this subsection, the sliding mode control laws for two subsystems are designed.

##### 3.1.1. ISM-based AMGST control for attitude subsystem

The control moment  $\mathbf{M}$  in attitude subsystem consists of two parts, that is,

$$\mathbf{M} = \mathbf{M}_s + \mathbf{M}_a, \quad (10)$$

where  $\mathbf{M}_s$  is designed in basis of ISM-based AMGST algorithm,  $\mathbf{M}_a$  is generated via ADP approach.

In this part, the design process of  $\mathbf{M}_s$  is introduced. First, define an integral sliding manifold as

$$\mathbf{S} = \mathbf{z}_\Theta - \int_0^t \mathbf{R}_\Theta \mathbf{I}^{-1} \mathbf{M}_a - \ddot{\Theta}_d d\tau. \quad (11)$$

The derivative of  $\mathbf{S}$  is

$$\dot{\mathbf{S}} = \mathbf{G}(\mathbf{z}_\Theta) + \mathbf{R}_\Theta \mathbf{I}^{-1} \mathbf{M}_s + \Delta_a + \Delta \dot{\mathbf{d}}_u. \quad (12)$$

According to (12),  $\mathbf{M}_s$  is designed as

$$\begin{aligned} \mathbf{M}_s &= \mathbf{I} \mathbf{R}_\Theta^{-1} (-k_1 \Phi_1(\mathbf{S}) + \mathbf{z}_1 - \mathbf{G}(\mathbf{z}_\Theta)) \\ \dot{\mathbf{z}}_1 &= -k_{20} L \Phi_2(\mathbf{S}), \end{aligned} \quad (13)$$

where  $\Phi_1(\mathbf{S}) = [\mathbf{S}]^{1/2} + \mathbf{S}$  and  $\Phi_2(\mathbf{S}) = \Phi_1' \Phi_1 = \frac{1}{2} [\mathbf{S}]^0 + \frac{3}{2} [\mathbf{S}]^{1/2} + \mathbf{S}$ ,  $k_1$  and  $L$  are adaptive gains, which are adapted

as

$$\dot{k}_1 = \begin{cases} \kappa_1 \|\mathbf{S}\| + \kappa_0, & \text{if } \|\mathbf{S}\| \neq 0 \\ 0, & \text{otherwise} \end{cases} \quad (14)$$

$$\begin{cases} L = L_0 + \Delta L \\ \Delta \dot{L} = -\lambda(t) \text{sign}(e_\Delta) \\ e_\Delta = 0.5L - \frac{1}{al} \|\bar{u}_{eq}\| - \varepsilon \\ \lambda(t) = \lambda_0 + r(t) \end{cases} \quad (15)$$

$$\dot{r}(t) = \begin{cases} \bar{r} |e_\Delta| \text{sign}(|e_\Delta| - \bar{e}), & r(t) > r_m \\ r_m, & \text{otherwise} \end{cases} \quad (16)$$

where  $k_{20}$ ,  $\kappa_1$ ,  $\kappa_0 \in (0, 1)$ ,  $\bar{e} \in (0, 1)$ ,  $L_0$ ,  $\bar{r}$ ,  $r_m$ ,  $\lambda_0$  are positive constants and  $0 < a < 1/l < 1$ ,  $\varepsilon$  is a small positive constant.  $\bar{u}_{eq}$ , which can be obtained by low-pass filtering the term  $\frac{k_{20}L}{2} [\mathbf{S}]^0$ , represents the approximate value of the equivalent control  $u_{eq}$ . It should be noted that the equivalent control  $u_{eq}$  is just theoretical control. The error between  $u_{eq}$  and its approximation  $\bar{u}_{eq}$  can be very small via selecting an appropriate time constant  $\tau$  [23, 46].

**Assumption 3.** For lumped disturbance  $\Delta_a$ , because it is related to the state  $\Theta$ , and  $\Phi_1(\mathbf{S})$  is a function associated with  $\Theta$  (since  $\mathbf{S}$  is related to  $\Theta$ ), it is reasonable to assume that there exists an unknown positive constant  $\delta_a$  to make  $\Delta_a$  satisfy  $\|\Delta_a\| \leq \delta_a \|\Phi_1(\mathbf{S})\|$ .

Substituting (13) into (12) yields

$$\begin{aligned} \dot{\mathbf{S}} &= -k_1 \Phi_1(\mathbf{S}) + \mathbf{z} + \Delta_a \\ \dot{\mathbf{z}} &= -k_{20} L \Phi_2(\mathbf{S}) + \Delta \dot{\mathbf{d}}_u \end{aligned} \quad (17)$$

where  $\mathbf{z} = \mathbf{z}_1 + \Delta \dot{\mathbf{d}}_u$ .

**Remark 2.** Since the attitude subsystem is a second-order MIMO system, we employ the multivariable generalized super-twisting algorithm. The multivariable design can avoid the necessity for the decoupled design with three SISO structures and it also exploits the coupling and inherent functional redundancy in fixed-wing UAV, which improves the safety of flight control.

Compared with standard super-twisting algorithm (STA), the generalized super-twisting algorithm (GSTA) can offer stronger robustness since the linear growth term in  $\Phi_1$  helps to counteract the state-dependent disturbance [47]. Furthermore, the two gains  $k_1$  and  $k_{20}L$  in  $\mathbf{M}_s$  are tuned via different gain-adaptation laws, respectively. The reason is that the disturbance  $\Delta_a$  and  $\Delta \dot{\mathbf{d}}_u$  are different, namely,  $\Delta_a$  is a state-dependent disturbance and  $\Delta \dot{\mathbf{d}}_u$  is just a time-dependent disturbance. The gain-adaptation law of  $k_1$  can counteract the state-dependent disturbance  $\Delta_a$ . Under the adjustment of gain-adaptation law (15)-(16),  $L$  changes with time-dependent disturbance  $\Delta \dot{\mathbf{d}}_u$  in real-time. Besides, compared to the adaptive-gain super-twisting (AST) in [21], the proposed AMGST

guarantees that the sliding mode manifold can converge to origin in finite time. However, the sliding variables under the AST can only converge to the finite domain of origin in theory.

**Remark 3.** The gain-adaptation law of  $r(t)$  is different from that in [23]. The overestimation of  $r(t)$  is considered in our work. Once the sliding mode associated with  $e_\Delta$  is achieved,  $r(t)$  shall start reducing and keep at a small level. Due to the decreasing of  $r(t)$ , the first-layer adaptive gain  $L$  will be smaller than that in [23].

**Theorem 1.** Consider system (6) with Assumptions 1-3. Let the integral sliding manifold  $\mathcal{S}$ , sliding mode control law  $\mathbf{M}_s$  and gain-adaptation law be designed as (11), (13), and (14)-(16), respectively. Then, the system (6) can reach the integral sliding manifold in finite time.

PROOF. For system (17), suppose that a gain-adaptation law has already been devised for updating  $L$  which is differentiable, bounded and satisfies  $L > \max\{L_0, 2\|\Delta\dot{d}_u\|\}$ . Under the above premise, we have  $L > 2\delta_{du1}$ . Define  $\eta = \frac{2\delta_{du1}}{L} \in (0, 1)$  and  $\mathbf{X} = [\mathbf{X}_1, \mathbf{X}_2]^T = [\Phi_1, \mathbf{z}]^T \in \mathbb{R}^6$ . The derivative of  $\mathbf{X}$  is

$$\begin{bmatrix} \dot{\mathbf{X}}_1 \\ \dot{\mathbf{X}}_2 \end{bmatrix} = -p_e \mathbf{A}_x \otimes \mathbf{I}_3 \begin{bmatrix} \mathbf{X}_1 \\ \mathbf{X}_2 \end{bmatrix}, \quad (18)$$

$$\text{where } \mathbf{A}_x = \begin{bmatrix} k_1 - \frac{\Delta_a^T \text{sign}(\Phi_1)}{\|\Phi_1\|} & -1 \\ k_{20}L - \frac{\Delta_a^T \text{sign}(\Phi_2)}{\|\Phi_2\|} & 0 \end{bmatrix}, p_e = \mathbf{X}'_1 =$$

$$\Phi'_1 = \frac{1}{2\|\mathcal{S}\|^{1/2}} + 1, \text{ and } \left| \frac{1}{p_e} \right| \leq 1.$$

To examine the stability of (18), a Lyapunov candidate is selected as

$$V_X = V_{X0} + \frac{(k_1 - \bar{k}_1)^2}{2\Gamma}, \quad (19)$$

where  $V_{X0} = \frac{1}{2}\mathbf{X}^T \mathbf{P} \mathbf{X}$ ,  $\Gamma > 0$ , and  $\mathbf{P} = \begin{bmatrix} p_1 & -1 \\ -1 & p_2 \end{bmatrix} \otimes \mathbf{I}_3 = \bar{\mathbf{P}} \otimes \mathbf{I}_3$  with  $p_1 > 0$ ,  $p_1 p_2 > 1$ . According to Proposition 1,  $\mathbf{P}$  is positive definite.  $\bar{k}_1$  is the upper bound of  $k_1$  (the boundedness of  $k_1$  will be analyzed later). The proof of Lyapunov candidate  $V_X$  is divided into two steps.

*Step 1:* The stability of  $V_{X0}$  is analyzed. Taking derivative of  $V_{X0}$ , we have

$$\dot{V}_{X0} = -p_e \mathbf{X}^T \mathbf{Q} \mathbf{X}, \quad (20)$$

where  $\mathbf{Q} = \mathbf{A}_x^T \mathbf{P} + \mathbf{P} \mathbf{A}_x = \begin{bmatrix} q_1 & q_2 \\ q_2 & q_3 \end{bmatrix} \otimes \mathbf{I}_3$  and

$$q_1 = \bar{k}_1 p_1 - \bar{k}_2,$$

$$q_2 = \frac{1}{2}(-p_1 - \bar{k}_1 + p_2 \bar{k}_2),$$

$$q_3 = 1$$

with  $\bar{k}_1 = k_1 - \frac{\Delta_a^T \text{sign}(\Phi_1)}{\|\Phi_1\|}$  and  $\bar{k}_2 = k_{20}L - \frac{\Delta_a^T \text{sign}(\Phi_2)}{\|\Phi_2\|}$ . Noting the fact that  $\left| \frac{1}{p_e} \right| \leq 1$  and  $\left\| \frac{1}{\Phi_2} \right\| \leq 2$ , the value ranges of  $\bar{k}_1$  and  $\bar{k}_2$  are deduced, that is,

$$\bar{k}_1 \in [\bar{k}_{1m}, \bar{k}_{1M}] = [k_1 - \delta_a, k_1 + \delta_a],$$

$$\bar{k}_2 \in [\bar{k}_{2m}, \bar{k}_{2M}] = [k_{20}L - 2\delta_{du1}, k_{20}L + 2\delta_{du1}].$$

To make  $\dot{V}_{E0}$  negative definite,  $\mathbf{Q}$  should satisfy

$$k_1 > \frac{\frac{k_{20}}{\eta} + 1}{\frac{p_1}{2\delta_{du1}}} + \delta_a, \quad (21)$$

$$-\frac{1}{4}p_1^2 + \frac{1}{2}(\bar{k}_1 + p_2 \bar{k}_2)p_1 - \bar{k}_2 - \frac{1}{4}(\bar{k}_1 - p_2 \bar{k}_2)^2 > 0. \quad (22)$$

(22) can be regard as a quadratic equation with respect to  $p_1$ . To make  $\mathbf{Q}$  positive definite, the discriminant of (22), i.e.,  $\Delta_Q = \bar{k}_2(p_2 \bar{k}_1 - 1)$ , has to be greater than zero. Thus, we have

$$k_{20} > \eta, \quad (23)$$

$$k_1 > \frac{1}{p_2} + \delta_a, \quad (24)$$

and the solution of inequality (22) is

$$p_1 \in (p_-, p_+) = \left( \bar{k}_1 + p_2 \bar{k}_2 - 2\sqrt{\Delta_Q}, \bar{k}_1 + p_2 \bar{k}_2 + 2\sqrt{\Delta_Q} \right).$$

To ensure  $p_1 \in (p_-, p_+)$  is a non-empty intersection set, the following condition has to be satisfied.

$$\begin{aligned} & \bar{k}_{1M} + p_2 \bar{k}_{2M} - 2\sqrt{\bar{k}_{2m}(p_2 \bar{k}_{1m} - 1)} < \\ & \bar{k}_{1m} + p_2 \bar{k}_{2m} + 2\sqrt{\bar{k}_{2m}(p_2 \bar{k}_{1m} - 1)}. \end{aligned} \quad (25)$$

Through several algebraic manipulations of (25), we deduce

$$k_1 > \frac{k_\varepsilon + 1}{p_2} + \delta_a \quad (26)$$

with  $k_\varepsilon = \frac{\frac{\delta_a^2}{2\delta_{du1}} + 2\delta_a p_2 + 2p_2^2 \delta_{du1}}{4(\frac{k_{20}}{\eta} - 1)}$ . When  $k_1$  satisfies

$$k_1 > \max \left[ \frac{\frac{k_{20}}{\eta} + 1}{\frac{p_1}{2\delta_{du1}}}, \frac{k_\varepsilon + 1}{p_2} \right] + \delta_a, \quad (27)$$

$\dot{V}_{X0}$  is negative definite.

Following the above analysis, we deduce that  $\mathbf{Q}$  is positive definite when  $k_{20}$  and  $k_1$  satisfy (23) and (27) and have

$$\lambda_{\min}(\mathbf{Q}) \|\mathbf{X}\|^2 \leq \mathbf{X}^T \mathbf{Q} \mathbf{X} \leq \lambda_{\max}(\mathbf{Q}) \|\mathbf{X}\|^2.$$

Noting the fact that  $\|\mathbf{X}_1\| \leq \|\mathbf{X}\|$  and  $\lambda_{\min}(\mathbf{P}) \|\mathbf{X}\|^2 \leq \mathbf{X}^T \mathbf{P} \mathbf{X} \leq \lambda_{\max}(\mathbf{P}) \|\mathbf{X}\|^2$ , (20) can be transformed into

$$\dot{V}_{X0} \leq -v_1 V_{X0}^{1/2} - v_2 V_{X0} \quad (28)$$

with  $v_1 = \frac{\lambda_{\min}(\mathbf{Q})\sqrt{\lambda_{\min}(\mathbf{P})}}{2\lambda_{\max}(\mathbf{P})}$  and  $v_2 = \frac{\lambda_{\min}(\mathbf{Q})}{\lambda_{\max}(\mathbf{P})}$ . Following the Theorem 4.2 in [48] and the assumption of  $L$ , if  $k_1$  and  $k_{20}$  are selected to satisfy (27) and (23), the system (18) is finite-time stable.

From the result in (28), the stability of  $V_X$  is analyzed. Under the condition that the initial value of  $k_1$  is greater than  $k_m$ , the derivative of (19) is

$$\begin{aligned}\dot{V}_X &\leq -v_1 V_{X0}^{1/2} - v_2 V_{X0} + \frac{1}{\Gamma}(k_1 - \bar{k}_1)(\kappa_1 \|\mathbf{S}\| + \kappa_0) \\ &\quad + \beta_K |k_1 - \bar{k}_1| - \beta_K |k_1 - \bar{k}_1| + \frac{\bar{k}_1}{\Gamma} \kappa_1 \|\mathbf{S}\| \\ &\quad + \beta_M |k_1 - \bar{k}_1| \bar{k}_1 - \beta_M (k_1 - \bar{k}_1)^2 - \frac{k_1}{\Gamma} \kappa_1 \|\mathbf{S}\| \\ &\leq -v_3 V_X^{1/2} - v_4 V_X - \zeta |k_1 - \bar{k}_1|,\end{aligned}\quad (29)$$

where  $\beta_K > 0$ ,  $\beta_M > 0$ ,  $v_3 = \min\{v_1, \beta_K\}$ ,  $v_4 = \min\{v_2, \beta_M\}$ , and

$$\zeta = -\beta_K + \frac{\kappa_0}{\Gamma} - \beta_M \bar{k}_1.$$

There always exists  $\Gamma = \frac{\kappa_0}{\beta_K + \beta_M \bar{k}_1}$ , which yields  $\zeta = 0$ . Then, inequality (29) is rewritten as

$$\dot{V}_X \leq -v_3 V_X^{1/2} - v_4 V_X, \quad (30)$$

which means that  $\mathbf{S}$  can converge to the origin in finite time.

It is worth noting that for the finite time convergence,  $k_1$  and  $k_{20}$  must satisfy inequality (27) and (23) under the assumption  $L > \max\{L_0, 2\|\Delta\ddot{d}_u\|\}$ . Namely, when  $\|\mathbf{S}\| \neq 0$ ,  $k_1$  will increase at the rate  $(\kappa_1 \|\mathbf{S}\| + \kappa_0)$  until the condition (27) is satisfied. Then,  $\|\mathbf{S}\|$  can converge in finite time.

According to the above analysis, it can be concluded that  $k_1$  is not monotonically increasing all the time. When  $\|\mathbf{S}\|$  converges to the origin,  $\dot{k}_1$  is equal to 0 and then  $k_1$  will remain unchanged. Therefore,  $k_1$  is bounded by a positive constant  $\bar{k}_1$ . The boundedness of  $k_1$  is ensured.

*Step 2:* In this step, the stability of adaptive gain  $L$  is analyzed. On the reaching phase,  $L < 2\delta_{du1}$  and then we have  $2\|\bar{u}_{eq}\| > L$ . Thus, there exists

$$e_\Delta = 0.5L - \frac{1}{al} \|\bar{u}_{eq}\| - \varepsilon < 0.$$

Obviously,  $\Delta\dot{L} > 0$  and  $L$  will increase at the rate  $\lambda(t)$ . After  $T \leq t_0 + \frac{2\delta_{du1} - L_0}{\lambda_0}$ ,  $L$  will be greater than  $2\delta_{du1}$ .

Now consider the following Lyapunov function.

$$V_L = \frac{1}{2}e_\Delta^2 + \frac{1}{2\Gamma_l}(r - r^*)^2, \quad (31)$$

where  $r^*$  represents the upper bound of  $r$  and  $\Gamma_l$  is an appropriate positive constant. In view of (15) and (16), it is easy to deduce that

$$\begin{aligned}\dot{V}_L &\leq -v_l |e_\Delta| - \beta_l |r - r^*| + \beta_l |r - r^*| \\ &\quad - \frac{1}{\Gamma_l} |r - r^*| \bar{r} |e_\Delta| \text{sign}(|e_\Delta| - \bar{e})\end{aligned}\quad (32)$$

with  $v_l = 0.5(\lambda_0 + r) - \frac{1}{al}\delta_{du2}$  and  $\beta_l > 0$ . There exists a condition that  $\lambda_0 + r > \frac{2}{al}\delta_{du2}$  to make sure  $v_l > 0$ . Define  $\varsigma_l = -(\beta_l - \frac{1}{\Gamma_l}\bar{r}|e_\Delta| \text{sign}(|e_\Delta| - \bar{e}))$  and we deduce

$$\dot{V}_L \leq -\bar{v}_l V_L^{1/2} - \varsigma_l |r - r^*|. \quad (33)$$

where  $\bar{v}_l = \min\{v_l, \beta_l\}$ . When  $|e_\Delta| > \bar{e}$ ,  $r$  will increase. If  $\Gamma_l < \frac{\bar{r}\bar{e}}{\beta_l}$ ,  $\varsigma_l$  will be positive and then the inequality  $\dot{V}_L \leq -\bar{v}_l V_L^{1/2}$  holds. According to the Theorem 4.2 in [48],  $e_\Delta$  can converge to the prescribed small interval  $|e_\Delta| < \bar{e}$  in finite time. When  $|e_\Delta| < \bar{e}$ ,  $\varsigma_l$  is negative, which results in the sign indefinite of  $\dot{V}_L$ .  $r$  will decrease and  $e_\Delta$  may increase. The process will go back to the case that  $|e_\Delta| > \bar{e}$ . Accordingly,  $e_\Delta$  is restricted to a finite domain of origin, namely,  $|e_\Delta| < \bar{e}_1$  with  $\bar{e}_1 > \bar{e}$ .

The proof of Theorem 1 is completed.

Following Theorem 1, the state trajectory of system (6) reaches the sliding manifold  $\mathcal{S}$  under the control law (13). According to (12) and  $\mathcal{S} = 0$ , the equivalent control law is

$$\mathbf{M}_{seq} = -\mathbf{I}\mathbf{R}_\Theta^{-1}(\Delta\dot{d}_u + \Delta_a + \mathbf{G}(\mathbf{z}_\Theta)).$$

Substituting  $\mathbf{M}_{seq}$  into (6), we derive

$$\begin{aligned}\dot{e}_\Theta &= \mathbf{z}_\Theta \\ \dot{\mathbf{z}}_\Theta &= \mathbf{R}_\Theta \mathbf{I}^{-1} \mathbf{M}_a - \ddot{\Theta}_d.\end{aligned}\quad (34)$$

Define  $\mathbf{E} = [e_\Theta^T, \mathbf{z}_\Theta^T]^T \in \mathbb{R}^6$ ,  $\mathbf{F}(\mathbf{z}_\Theta) = [\mathbf{z}_\Theta^T, \mathbf{0}_{1 \times 3}]^T \in \mathbb{R}^6$ ,  $\ddot{\Theta}_d = [\mathbf{0}_{1 \times 3}, \ddot{\Theta}_d^T]^T \in \mathbb{R}^6$ , and  $\bar{\mathbf{g}} = [\mathbf{0}_{3 \times 3}, (\mathbf{R}_\Theta \mathbf{I}^{-1})^T]^T \in \mathbb{R}^{6 \times 3}$ . (34) is rewritten as

$$\dot{\mathbf{E}} = \mathbf{F}(\mathbf{z}_\Theta) + \bar{\mathbf{g}} \mathbf{M}_a - \ddot{\Theta}_d. \quad (35)$$

According to (34) and (35),  $\Delta_a$  and  $\Delta d_u$  are completely compensated by  $\mathbf{M}_s$ . Without the effect of time-varying disturbances, the optimal control problem for system (35) can be regard as time-invariant, and then the ADP approach is used to design  $\mathbf{M}_a$ , whose design process is shown in Subsection 3.2.

### 3.1.2. ISM-based AGST control for airspeed subsystem

Similar to the design of  $\mathbf{M}$  in attitude subsystem, the thrust  $T_x$  is also composed of two parts, namely,

$$T_x = T_{xs} + T_{xa}, \quad (36)$$

where  $T_{xs}$  is generated via the ISM-based AGST algorithm.  $T_{xa}$  is generated via ADP approach. The design process of  $T_{xs}$  is detailed in this part. First, the ISM of airspeed subsystem is designed as

$$S_V = e_V(t) - \int_0^t -g_v - \dot{V}_d + \frac{\cos \alpha \cos \beta T_{xa} - D}{m} d\tau. \quad (37)$$

Taking the derivative of  $S_V$ , we have

$$\dot{S}_V = \frac{\cos \alpha \cos \beta T_{xs}}{m} + \Delta_V \quad (38)$$

and  $T_{xs}$  is designed as

$$\begin{aligned} T_{xs} &= \frac{m}{\cos \alpha \cos \beta} \left( -k_{1v} \sqrt{\frac{L_v}{2}} \phi_{v1} + z_v \right. \\ &\quad \left. + \phi_{v3}(L_v, \phi_{v1}) \right) \\ \dot{z}_v &= -k_{2v} L_v \phi_{v2} \end{aligned} \quad (39)$$

with  $\phi_{v1} = [S_V]^{1/2} + S_V$ ,  $\phi_{v2} = \phi'_{v1} \phi_{v1} = \frac{1}{2} [S_V]^0 + \frac{3}{2} [S_V]^{1/2} + S_V$ , and  $\phi_{v3}(L_v, \phi_{v1}) = -\frac{\dot{L}_v \phi_{v1}}{2L_v \phi'_{v1}}$ . The derivative of  $\phi_{v1}$  with respect to  $S_V$  is  $\phi'_{v1} = \frac{1}{2} |S_V|^{-1/2} + 1$ . To ease the notation, we denote  $\phi_{v3}(L_v, \phi_{v1}) = \phi_{v3}$ .  $k_{1v}$  and  $k_{2v}$  are positive constants.  $L_v$  is adaptive gain and adjusted via the following gain-adaptation law

$$\begin{cases} L_v = L_{v0} + \Delta L_v \\ \Delta \dot{L}_v = -\lambda_v(t) \text{sign}(\bar{e}_v) \\ \bar{e}_v = 0.5L_v - \frac{1}{l_v} |\bar{u}_{eqv}| - \varepsilon_v \\ \lambda_v(t) = \lambda_{v0} + r_v(t) \end{cases} \quad (40)$$

$$\dot{r}_v(t) = \begin{cases} \bar{r}_v |\bar{e}_v| \text{sign}(|\bar{e}_v| - e_b), & r_v(t) > r_{mv} \\ r_{mv}, & \text{otherwise} \end{cases}, \quad (41)$$

where  $L_{v0}$ ,  $\lambda_{v0}$ ,  $\bar{r}_v$ ,  $e_b$ , and  $r_{mv}$  are positive constants and  $0 < 1/l_v < 1$ .  $\varepsilon_v$  is small positive constant.  $\bar{u}_{eqv}$  is the close approximation of equivalent control  $u_{eqv}$ , which is obtained by the following low-pass filter

$$\dot{\bar{u}}_{eqv} = \frac{1}{\tau} \left[ \frac{k_{2v} L_v}{2} [S_V]^0 - \bar{u}_{eqv} \right], \quad (42)$$

where time constant  $\tau$  is set to be small enough so that  $\bar{u}_{eqv}$  can be close to  $u_{eqv}$  arbitrarily [23, 46].

Substituting control law (39) into (38) yields

$$\begin{aligned} \dot{S}_V &= -k_{1v} \sqrt{\frac{L_v}{2}} \phi_{v1} + \bar{z}_v + \phi_{v3} \\ \dot{\bar{z}}_v &= -k_{2v} L_v \phi_{v2} + \dot{\Delta}_V \end{aligned} \quad (43)$$

with  $\bar{z}_v = z_v + \Delta_V$ .

**Remark 4.**  $\phi_{v3}$  is an adaptation term used to ensure the stability of system (43). When  $\phi_{v3} \neq 0$ ,  $\phi_{v3}$  is an acceleration term, which improves the convergence speed. When  $\dot{L}_v$  is equal to 0 or  $S_V$  converges to 0 ( $\phi_{v1}$  is also equal to 0),  $\phi_{v3} = 0$  and the controller (39) reverts to the traditional generalized super-twisting structure.

**Remark 5.** The gain-adaptation laws designed for attitude and airspeed subsystem are different (see (14)-(16) and (40)-(41)). For airspeed subsystem, because there only exists time-dependent disturbance  $\Delta_V$ , the two gains in (39) are both adjusted via the gain-adaptation law (40)-(41). The parameter selection of this design is simple. Under the adjustment of (40)-(41), the two gains of controller (39) are updated in real-time according to the change of disturbance, which can attenuate the chattering efficiently.

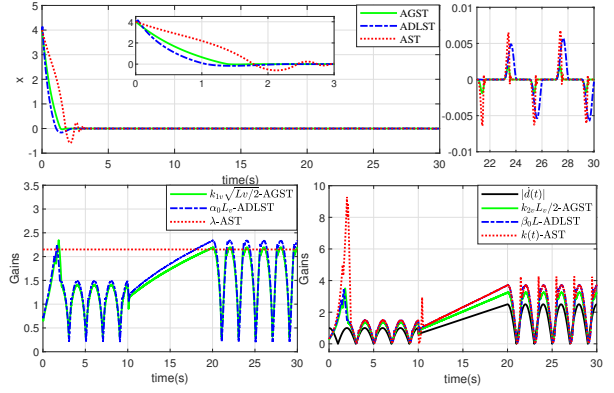


Figure 2: State  $x$  and control gains.

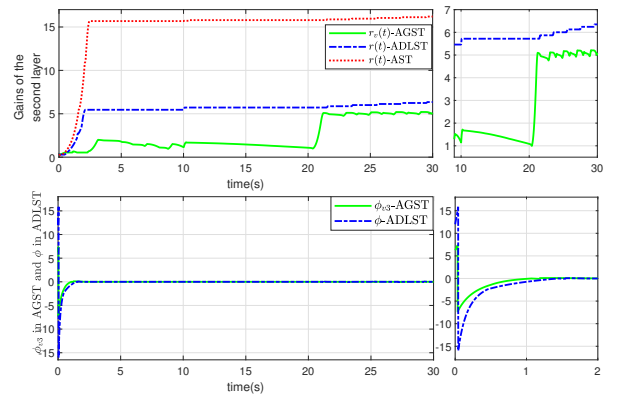


Figure 3: The second-layer gains in three control algorithms and  $\phi_{v3}$ ,  $\phi$  in AGST, ADLST.

In comparison with the adaptive-gain super-twisting (AST) in [23] and adaptive dual-layer super-twisting (ADLST) in [24], the proposed AGST has better control performance when facing unknown disturbance. The comparative results shown in Figs. 2 and 3 illustrate this. For SISO system  $\dot{x} = u + d(t)$ ,  $x$  is the state and  $u$  is the control input. The disturbance  $d(t)$  is given as

$$d(t) = \begin{cases} \frac{2 \sin(0.5\pi t)}{\pi}, & 0 \leq t < 10 \\ \frac{3}{32} t^2 - \frac{5}{4} t, & 10 \leq t < 20 \\ \frac{3 \sin(0.5\pi t)}{\pi}, & 20 \leq t < 30 \end{cases}.$$

The parameters setting of (40)-(41) is  $k_{1v} = 1.35$ ,  $k_{2v} = 1.26$ ,  $L_{v0} = 0.26$ ,  $l_v = 0.99$ ,  $\varepsilon_v = 0.05$ ,  $\lambda_{v0} = 0.38$ ,  $\bar{r}_v = 7$ ,  $e_b = 0.15$ , and  $r_{mv} = 0.6$ . The parameters setting of ADLST in [24] is  $\alpha_0 = 1.35$ ,  $\beta_0 = 1.26$ ,  $a\beta_0 = 0.99$ ,  $\varepsilon = 0.05$ ,  $l_0 = 0.26$ ,  $\gamma = 7$ , and  $r_0 = 0.38$ . The parameters setting of gain-adaptation law of AST [23] is same as that of ADLST and the fixed gain  $\lambda$  is set as 2.2. The specific definition of parameters in ADLST and AST can refer to [24] and [23].

The results in Fig. 2 show that the AGST has smaller overshoot and convergence time compared with other two algorithms. The convergence precision of AGST is also higher

than the other two algorithms.  $\frac{k_{2v}L_v}{2}$ ,  $\beta_0L$ , and  $k(t)$  change with  $|d(t)|$  in real time, but the value of  $\frac{k_{2v}L_v}{2}$  is smaller than  $\beta_0L$  and  $k(t)$  because the second-layer control gain  $r_v(t)$  decreases after 10s and fluctuates around 5 after 20s (see the top sub-graph of Fig. 3). The modified gain-adaptation law in (40) and (41) can avoid the overestimation of control gain  $L_v$  and  $r_v$  better, which will alleviate the chattering more effectively. In addition, the results in Fig. 3 indicate that the adaptation term  $\phi_{v3}$  helps to achieve faster convergence speed in the initial phase, which confirm the descriptions in Remark 4.

**Theorem 2.** For system (8) with Assumption 2, design the integral sliding manifold  $S_V$  (37) and sliding mode control law  $T_{xs}$  (39) with gain-adaptation law (40)-(41). Then, the system trajectory can reach the integral sliding manifold  $S_V$  in finite time.

PROOF. The stability analysis of system (43) consists of two steps.

*Step 1:* Define  $\mathbf{X}_v = [X_{v1}, X_{v2}]^T = [\sqrt{\frac{L_v}{2}}\phi_{v1}, \bar{z}_v]^T$  and the derivative of  $\mathbf{X}_v$  is

$$\dot{\mathbf{X}}_v = \sqrt{L_v}\phi'_{v1}(\mathbf{A}_{v0}\mathbf{X}_v + \mathbf{B}_{v0}\tilde{\Delta}_V), \quad (44)$$

with  $\tilde{\Delta}_V = \frac{\Delta_V}{\sqrt{L_v}\phi'_{v1}}$ ,  $\mathbf{A}_{v0} = \sqrt{2} \begin{bmatrix} -\frac{k_{1v}}{2} & \frac{1}{2} \\ -k_{2v} & 0 \end{bmatrix}$ , and  $\mathbf{B}_{v0} = [0, 1]^T$ .

Similar to the proof process of Theorem 1, suppose that there has been a gain-adaptation law to tune  $L_v$  and ensure  $L_v > \max\{L_{v0}, 2|\dot{\Delta}_V|\}$ . Further, from Assumption 2, we have  $L_v > 2\delta_{V0}$ . For system (44), a Lyapunov function candidate is selected as

$$V_{v0} = \frac{1}{2}\mathbf{X}_v^T \mathbf{P}_v \mathbf{X}_v, \quad (45)$$

where  $\mathbf{P}_v = \begin{bmatrix} \varpi_1 & -1 \\ -1 & \varpi_2 \end{bmatrix}$  is a positive definite matrix with  $\varpi_1 > 0$  and  $\varpi_1\varpi_2 > 1$ . The goal of Step 1 is to obtain the stability condition of  $k_{1v}$  and  $k_{2v}$  such that the finite-time stability of system (43) can be obtained.

Taking the derivative of  $V_{v0}$  with respect to time yields

$$\begin{aligned} \dot{V}_{v0} &= \frac{1}{2}\sqrt{L_v}\phi'_{v1}(\mathbf{X}_v^T \mathbf{A}_{v0}^T \mathbf{P}_v \mathbf{X}_v + \mathbf{X}_v^T \mathbf{P}_v \mathbf{A}_{v0} \mathbf{X}_v \\ &\quad + 2\mathbf{X}_v^T \mathbf{P}_v \mathbf{B}_{v0} \tilde{\Delta}_V) \\ &\leq \frac{1}{2}\sqrt{L_v}\phi'_{v1}(\mathbf{X}_v^T \mathbf{A}_{v0}^T \mathbf{P}_v \mathbf{X}_v + \mathbf{X}_v^T \mathbf{P}_v \mathbf{A}_{v0} \mathbf{X}_v \\ &\quad + \mathbf{X}_v^T \mathbf{P}_v \mathbf{B}_{v0} \mathbf{B}_{v0}^T \mathbf{P}_v \mathbf{X}_v + \tilde{\Delta}_V^2). \end{aligned} \quad (46)$$

$$\text{From } \tilde{\Delta}_V = \frac{\Delta_V}{\sqrt{L_v}(\frac{1}{2}|S_V|^{-\frac{1}{2}}+1)},$$

$$|\tilde{\Delta}_V| \leq \frac{2\sqrt{2}|\dot{\Delta}_V|}{L_v} \|\mathbf{X}_v\|. \quad (47)$$

Because we have supposed that  $L_v > \max\{L_{v0}, 2|\dot{\Delta}_V|\}$ ,  $|\tilde{\Delta}_V| < \sqrt{2}\|\mathbf{X}_v\|$  and (46) is transformed into

$$\begin{aligned} \dot{V}_{v0} &\leq \frac{1}{2}\sqrt{L_v}\phi'_{v1} \mathbf{X}_v^T (\mathbf{A}_{v0}^T \mathbf{P}_v + \mathbf{P}_v \mathbf{A}_{v0} + \mathbf{C}_{v0}^T \mathbf{C}_{v0} \\ &\quad + \mathbf{P}_v \mathbf{B}_{v0} \mathbf{B}_{v0}^T \mathbf{P}_v) \mathbf{X}_v \\ &= -\frac{1}{2}\sqrt{L_v}\phi'_{v1} \mathbf{X}_v^T \mathbf{Q}_{v0} \mathbf{X}_v, \end{aligned}$$

where  $\mathbf{C}_{v0} = [\sqrt{2}, 0]^T$  and  $\mathbf{Q}_{v0} = -(\mathbf{A}_{v0}^T \mathbf{P}_v + \mathbf{P}_v \mathbf{A}_{v0} + \mathbf{C}_{v0}^T \mathbf{C}_{v0} + \mathbf{P}_v \mathbf{B}_{v0} \mathbf{B}_{v0}^T \mathbf{P}_v)$ . To ensure the negative definite of  $\dot{V}_{v0}$ , following condition has to be satisfied.

$$\mathbf{A}_{v0}^T \mathbf{P}_v + \mathbf{P}_v \mathbf{A}_{v0} + \mathbf{C}_{v0}^T \mathbf{C}_{v0} + \mathbf{P}_v \mathbf{B}_{v0} \mathbf{B}_{v0}^T \mathbf{P}_v < 0. \quad (48)$$

Then, noting that

$$\lambda_{\min}(\mathbf{Q}_{v0}) \|\mathbf{X}_v\|^2 \leq \mathbf{X}_v^T \mathbf{Q}_{v0} \mathbf{X}_v \leq \lambda_{\max}(\mathbf{Q}_{v0}) \|\mathbf{X}_v\|^2,$$

$$\lambda_{\min}(\mathbf{P}_v) \|\mathbf{X}_v\|^2 \leq \mathbf{X}_v^T \mathbf{P}_v \mathbf{X}_v \leq \lambda_{\max}(\mathbf{P}_v) \|\mathbf{X}_v\|^2,$$

we obtain

$$\dot{V}_{v0} \leq -v_{v1}V_{v0}^{1/2} - v_{v2}V_{v0} \quad (49)$$

with  $v_{v1} = \frac{L_{v0}\lambda_{\min}(\mathbf{Q}_{v0})\sqrt{\lambda_{\min}(\mathbf{P}_v)}}{4\lambda_{\max}(\mathbf{P}_v)}$  and  $v_{v2} = \frac{\sqrt{L_{v0}}\lambda_{\min}(\mathbf{Q}_{v0})}{\lambda_{\max}(\mathbf{P}_v)}$ . Based the Theorem 4.2 in [48] and the assumption of  $L_v$ , it can be concluded that the system (44) is finite-time stable via selecting appropriate  $k_{1v}$  and  $k_{2v}$  to satisfy (48).

*Step 2:* In Step 2, the stability of adaptive gain  $L_v$  is analyzed. Because the gain-adaptation law of  $L_v$  is similar to that of  $L$ , the proving process of (40)-(41) is simply introduced in this step. On the reaching phase,  $L_v$  is less than  $2\delta_{V0}$  and  $\bar{e}_v$  is negative. According to (40)-(41),  $L_v$  will increase until  $L_v > 2\delta_{V0}$ . To examine the stability of  $L_v$ , choose the Lyapunov function as

$$V_{L_v} = \frac{1}{2}\bar{e}_v^2 + \frac{1}{2\Gamma_v}(r_v - r_v^*)^2, \quad (50)$$

where  $r_v^*$  represents the upper bound of  $r_v$  and  $\Gamma_v > 0$ . The derivative of  $V_{L_v}$  is

$$\begin{aligned} \dot{V}_{L_v} &= \bar{e}_v \dot{\bar{e}}_v + \frac{1}{\Gamma_v}(r_v - r_v^*)\dot{r}_v \\ &\leq -\frac{1}{2}v_{v1}|\bar{e}_v| - \beta_{rv}|r_v - r_v^*| - \varsigma_{rv}|r_v - r_v^*|, \end{aligned} \quad (51)$$

where  $v_{v1} = \lambda_{v0} + r_v - \frac{2\delta_{V1}}{l_v}$ ,  $\beta_{rv} > 0$ , and  $\varsigma_{rv} = -\beta_{rv} + \frac{1}{\Gamma_v}\bar{r}_v|\bar{e}_v|\text{sign}(|\bar{e}_v| - e_b)$ . To guarantee the positiveness of  $v_{v1}$ , the condition  $\lambda_{v0} + r_v > \frac{2\delta_{V1}}{l_v}$  has to be satisfied. Based on the above condition, (51) is rewritten as  $\dot{V}_{L_v} \leq -\bar{v}_v V_{L_v}^{1/2} - \varsigma_{rv}|r_v - r_v^*|$  with  $\bar{v}_v = \min\{\frac{1}{2}v_{v1}, \beta_{rv}\}$ . When  $|\bar{e}_v| > e_b$ ,  $r_v$  will increase and  $\varsigma_{rv}$  is positive if

$$\Gamma_v < \frac{\bar{r}_v e_b}{\beta_{rv}}.$$



Then, inequality  $\dot{V}_{L_v} \leq -\bar{v}_v V_{L_v}^{1/2}$  holds, which illustrates that  $\bar{e}_v$  can converge to the domain  $|\bar{e}_v| < e_b$  in finite time [48]. Similar to the analysis process of  $e_\Delta$  in attitude subsystem,  $\bar{e}_v$  could be sustained in a bigger domain, i.e.,  $|\bar{e}_v| < e_{b1}$  with  $e_{b1} > e_b$ , and  $r_v$  has an upper bound  $r_v^*$ . Thereout, we can infer that the adaptive-gain  $L_v$  is also bounded.

The proof of Theorem 2 is completed.

When the system trajectory reach and maintain on the sliding manifold  $S_V$ , with (38) and  $\dot{S}_V = 0$ , the equivalent control  $T_{xse}$  is deduced as

$$T_{xse} = -\frac{m}{\cos \alpha \cos \beta} \Delta_V.$$

Substitute  $T_{xse}$  into (8) and then the sliding mode dynamic is written as

$$\dot{e}_V = \frac{\cos \alpha \cos \beta T_{xa} - D}{m} - g_v - \dot{V}_d. \quad (52)$$

From (52), the effect of unknown disturbance  $\Delta_V$  is completely compensated by the control law (39). Next, the ADP approach can be employed to generate  $T_{xa}$  such that the sliding mode dynamic (52) has a nearly optimal performance. The design process of  $T_{xa}$  is detailed in Subsection 3.2

### 3.2. Nearly optimal control design

With the analysis in Subsection 3.1, the tracking error systems (6) and (8) are converted to the equivalent sliding mode dynamics (35) and (52) when the system trajectories come to the ISMs. By combining the results in Subsection 3.1, the nearly optimal control laws  $\mathbf{M}_a$  and  $T_{xa}$  are designed via modified ADP approach in this subsection.

Define  $\mathbf{E}_V = [\mathbf{E}^T, e_V]^T \in \mathbb{R}^7$ ,  $\mathbf{F}_V(\mathbf{z}_\Theta) = [\mathbf{F}^T(\mathbf{z}_\Theta), -\frac{D}{m} - g_v]^T \in \mathbb{R}^7$ ,  $\mathbf{X}_d = [\bar{\Theta}_d^T, \dot{V}_d]^T \in \mathbb{R}^7$ ,  $\mathbf{U}_a = [\mathbf{M}_a^T, T_{xa}]^T \in \mathbb{R}^4$ , and  $\mathbf{G}_V = [\mathbf{0}_{4 \times 3}, \mathbf{G}_{V2}]^T \in \mathbb{R}^{7 \times 4}$  with

$$\mathbf{G}_{V2} = \begin{bmatrix} \mathbf{R}_\Theta \mathbf{I}^{-1} & \mathbf{0}_{3 \times 1} \\ \mathbf{0}_{1 \times 3} & \frac{\cos \alpha \cos \beta}{m} \end{bmatrix}^T.$$

Then, (35) and (52) can be transformed into

$$\dot{\mathbf{E}}_V = \mathbf{F}_V(\mathbf{z}_\Theta) + \mathbf{G}_V \mathbf{U}_a - \mathbf{X}_d. \quad (53)$$

**Assumption 4.** From the engineering viewpoint, suppose that a positive constant  $\delta_G$  can be found such that  $\|\mathbf{G}_V\| \leq \delta_G$ .

**Remark 6.** Through the expression of  $\mathbf{G}_V$ , we can observe that  $\mathbf{G}_V$  is a matrix which related to the trigonometric function of  $\Theta$ ,  $\alpha$ , and  $\beta$ . Since  $\theta$  cannot be equal to  $\pm \frac{\pi}{2}$  and then  $\tan \theta$  is bounded, the assumption  $\|\mathbf{G}_V\| \leq \delta_G$  is reasonable.

Based on (53), the nearly optimal control law  $\mathbf{U}_a$  is constructed. First, a infinite horizon performance index function  $V_a(\mathbf{E}_V)$  is defined as

$$V_a(\mathbf{E}_V) = \int_t^\infty r_V(\mathbf{E}_V, \mathbf{U}_a) d\tau \quad (54)$$

with  $r_V(\mathbf{E}_V, \mathbf{U}_a) = \bar{\mathbf{Q}}_E(\mathbf{E}_V) + \mathbf{U}_a^T \mathbf{R}_u \mathbf{U}_a$  and  $\bar{\mathbf{Q}}_E(\mathbf{E}_V) = \mathbf{E}_V^T \mathbf{Q}_E \mathbf{E}_V$ .  $\mathbf{Q}_E(\mathbf{E}_V) \in \mathbb{R}^{7 \times 7}$  is a positive-definite matrix.  $\mathbf{R}_u = \text{diag}\{R_{u1}, R_{u2}, R_{u3}, R_{u4}\} \in \mathbb{R}^{4 \times 4}$  is a symmetric positive definite matrix. For  $\bar{\mathbf{Q}}_E(\mathbf{E}_V)$ , a small positive constant  $b_E$  can be found such that  $\bar{\mathbf{Q}}_E(\mathbf{E}_V) \geq b_E \|\mathbf{E}_V\|^2$ .

Our aim is to obtain the optimal control law  $\mathbf{U}_a$  to minimize the performance index function  $V_a(\mathbf{E}_V)$  and stabilize the system (53).

Associated with (53) and (54), the Hamiltonian function is

$$H(\mathbf{E}_V, \mathbf{U}_a, \nabla V_a) = \nabla V_a (\mathbf{F}_V(\mathbf{z}_\Theta) + \mathbf{G}_V \mathbf{U}_a - \mathbf{X}_d) + \bar{\mathbf{Q}}_E(\mathbf{E}_V) + \mathbf{U}_a^T \mathbf{R}_u \mathbf{U}_a \quad (55)$$

with  $\nabla V_a = \frac{\partial V_a}{\partial \mathbf{E}_V}$ . The optimal control law is  $\mathbf{U}_a^*$  and the optimal performance index is

$$V_a^*(\mathbf{E}_V) = \int_t^\infty r_V(\mathbf{E}_V, \mathbf{U}_a^*) d\tau. \quad (56)$$

According to (56), the Hamilton-Jacobi-Bellman (HJB) equation is

$$H(\mathbf{E}_V, \mathbf{U}_a^*, \nabla V_a^*) = \nabla V_a^{*T} (\mathbf{F}_V(\mathbf{z}_\Theta) + \mathbf{G}_V \mathbf{U}_a^* - \mathbf{X}_d) + \bar{\mathbf{Q}}_E(\mathbf{E}_V) + \mathbf{U}_a^{*T} \mathbf{R}_u \mathbf{U}_a^* = 0 \quad (57)$$

with  $\nabla V_a^* = \frac{\partial V_a^*}{\partial \mathbf{E}_V}$ . Then,  $\mathbf{U}_a^*$  can be yielded as

$$\mathbf{U}_a^* = -\frac{1}{2} \mathbf{R}_u^{-1} \mathbf{G}_V^T \nabla V_a^* = [\mathbf{M}_a^{*T}, T_{xa}^*]^T, \quad (58)$$

and (57) is transformed into

$$H(\mathbf{E}_V, \mathbf{U}_a^*, \nabla V_a^*) = \nabla V_a^{*T} (\mathbf{F}_V(\mathbf{z}_\Theta) - \mathbf{X}_d) + \bar{\mathbf{Q}}_E(\mathbf{E}_V) - \frac{1}{4} \nabla V_a^{*T} \mathbf{G}_V \mathbf{R}_u^{-1} \mathbf{G}_V^T \nabla V_a^* = 0. \quad (59)$$

Through (58) and (59), the gradient  $\nabla V_a^*$  is achieved. Next, the optimal control law is obtained through  $\nabla V_a^*$ . Nevertheless, due to the strong nonlinearity, it is difficult or even impossible to solve the nonlinear HJB equation via analytical methods. Hence, a modified ADP approach based on the actor-critic (AC) structure is proposed to overcome the above difficulty.

**Design of Critic NN and Actor NN:** In the AC structure, the optimal control law  $\mathbf{U}_a^*$  and the optimal performance index  $V_a^*(\mathbf{E}_V)$  are approximated by actor neural network (ANN) and critic neural network (CNN), respectively.

In our work,  $V_a^*(\mathbf{E}_V)$  is divided into two parts, which is shown as

$$\begin{aligned} V_a^*(\mathbf{E}_V) &= \beta_w \|\mathbf{E}_V\|^2 - \beta_w \|\mathbf{E}_V\|^2 + V_a^*(\mathbf{E}_V) \\ &= \beta_w \|\mathbf{E}_V\|^2 + V_{a2}^*(\mathbf{E}_V), \end{aligned} \quad (60)$$

where  $\beta_w > 0$  and  $V_{a2}^*(E_V) = -\beta_w \|E_V\|^2 + V_a^*(E_V)$ . According to the Weierstrass high-order approximation theorem [40], there exist a neural network (NN) such that  $V_{a2}^*(E_V)$  is approximated as

$$V_{a2}^*(E_V) = \mathbf{W}_c^{*T} \boldsymbol{\sigma}_w(E_V) + \delta_w, \quad (61)$$

where  $\mathbf{W}_c^* = [W_{c1}^*, \dots, W_{cN}^*]^T$  is the optimal weight vector,  $N$  represents the number of neurons.  $\boldsymbol{\sigma}_w(E_V) = [\sigma_{w1}, \sigma_{w2}, \dots, \sigma_{wN}]^T$  is the suitable activation function vector and each elements in  $\boldsymbol{\sigma}_w(E_V)$  is selected to be linearly independent.  $\delta_w$  is the approximation error. Substituting (61) into (60) yields

$$V_a^*(E_V) = \beta_w \|E_V\|^2 + \mathbf{W}_c^{*T} \boldsymbol{\sigma}_w(E_V) + \delta_w \quad (62)$$

and  $\nabla V_a^*$  is

$$\nabla V_a^* = 2\beta_w E_V + \nabla \boldsymbol{\sigma}_w^T \mathbf{W}_c^* + \nabla \delta_w \quad (63)$$

where  $\nabla \boldsymbol{\sigma}_w = \frac{\partial \boldsymbol{\sigma}_w(E_V)}{\partial E_V}$  and  $\nabla \delta_w = \frac{\partial \delta_w}{\partial E_V}$ .

**Assumption 5.** According to the universal approximation principle, the approximation error  $\delta_w$  and its gradient are bounded, i.e.,  $\|\delta_w\| \leq \bar{\delta}_w$  and  $\|\nabla \delta_w\| \leq \bar{\delta}_{w0}$  with  $\bar{\delta}_w > 0$ ,  $\bar{\delta}_{w0} > 0$ . Besides, activation function vector  $\boldsymbol{\sigma}_w(E)$  and its gradient are also bounded, i.e.,  $\|\boldsymbol{\sigma}_w(E_V)\| \leq \bar{\delta}_\sigma$  and  $\|\nabla \boldsymbol{\sigma}_w\| \leq \bar{\delta}_{\sigma 0}$  with  $\bar{\delta}_\sigma > 0$ ,  $\bar{\delta}_{\sigma 0} > 0$  [42, 49].

Substituting (63) into (58), rewrite the optimal control law  $U_a^*$  as

$$U_a^* = -\frac{1}{2} \mathbf{R}_u^{-1} \mathbf{G}_V^T (2\beta_w E_V + \nabla \boldsymbol{\sigma}_w^T \mathbf{W}_c^*) + \delta_{wu} \quad (64)$$

where  $\delta_{wu}$  is the approximation error of the optimal control law.  $\delta_{wu}$  is relevant to  $\delta_w$  and satisfies  $\|\delta_{wu}\| \leq \bar{\delta}_{wu}$ ,  $\bar{\delta}_{wu} > 0$ .

According to (63) and (64), HJB equation is derived as

$$\begin{aligned} H(E_V, U_a^*, \nabla V_a^*) &= (2\beta_w E_V + \nabla \boldsymbol{\sigma}_w^T \mathbf{W}_c^*)(F_V(\mathbf{z}_\Theta) \\ &- X_d) + \bar{\mathbf{Q}}_E(E_V) - \frac{1}{4} (2\beta_w E_V + \nabla \boldsymbol{\sigma}_w^T \mathbf{W}_c^*)^T \mathbf{G}_V \\ &\cdot \mathbf{R}_u^{-1} \mathbf{G}_V^T (2\beta_w E_V + \nabla \boldsymbol{\sigma}_w^T \mathbf{W}_c^*) - \delta_{HJB} = 0 \end{aligned} \quad (65)$$

where  $\delta_{HJB}$  is the residual error and related to the approximation error  $\delta_w$  and  $\delta_{wu}$ . A positive constant can be found such that  $\|\delta_{HJB}\| \leq \bar{\delta}_h$ .

Sine the ideal weight vector is unknown, the CNN and ANN are constructed as follows.

$$\hat{V}_a(E_V) = \beta_w \|E_V\|^2 + \hat{\mathbf{W}}_c^T \boldsymbol{\sigma}_w(E_V), \quad (66)$$

$$\begin{aligned} \hat{U}_a &= -\frac{1}{2} \mathbf{R}_u^{-1} \mathbf{G}_V^T (2\beta_w E_V + \nabla \boldsymbol{\sigma}_w^T \hat{\mathbf{W}}_a) \\ &= [\mathbf{M}_a^T, T_{xa}]^T, \end{aligned} \quad (67)$$

and  $\nabla \hat{V}_a$  is

$$\nabla \hat{V}_a = 2\beta_w E_V + \nabla \boldsymbol{\sigma}_w^T \hat{\mathbf{W}}_c^T, \quad (68)$$

where  $\nabla \boldsymbol{\sigma}_w^T = \frac{\partial \boldsymbol{\sigma}_w(E_V)}{\partial E_V}$ .  $\hat{\mathbf{W}}_c$  and  $\hat{\mathbf{W}}_a$  are the weight vectors of CNN and ANN, respectively. It is obvious that  $\hat{\mathbf{W}}_c$  and  $\hat{\mathbf{W}}_a$  are used to approximate the same ideal  $\mathbf{W}_c^*$ .

From (67) and (68), the HJB equation is given by

$$\begin{aligned} \hat{H}(E_V, \hat{U}_a, \nabla \hat{V}_a) &= (2\beta_w E_V + \nabla \boldsymbol{\sigma}_w^T \hat{\mathbf{W}}_c)(F_V(\mathbf{z}_\Theta) \\ &+ \mathbf{G}_V \hat{U}_a - X_d) + \bar{\mathbf{Q}}_E(E_V) + \hat{U}_a^T \mathbf{R}_u \hat{U}_a, \end{aligned} \quad (69)$$

and the Bellman residual error  $\Delta_B$  is

$$\begin{aligned} \Delta_B &= \hat{H}(E_V, \hat{U}_a, \nabla \hat{V}_a) - H(E_V, U_a^*, \nabla V_a^*) \\ &= \hat{H}(E_V, \hat{U}_a, \nabla \hat{V}_a). \end{aligned} \quad (70)$$

To minimize the Bellman residual error  $\Delta_B$ , define a objective function as  $E_c = \frac{1}{2} \Delta_B^T \Delta_B$ .  $\hat{\mathbf{W}}_c$  and  $\hat{\mathbf{W}}_a$  are updated to minimize  $E_c$ . Based on the gradient descent method, the updating law of  $\hat{\mathbf{W}}_c$  is obtained as

$$\begin{aligned} \dot{\hat{\mathbf{W}}}_c &= -c_0 \frac{m_w}{(1+m_w^T m_w)^2} [(2\beta_w E_V + \nabla \boldsymbol{\sigma}_w^T \hat{\mathbf{W}}_c)(F_V(\mathbf{z}_\Theta) \\ &+ \mathbf{G}_V \hat{U}_a - X_d) + \bar{\mathbf{Q}}_E(E_V) + \hat{U}_a^T \mathbf{R}_u \hat{U}_a]. \end{aligned} \quad (71)$$

According to the stability analysis, the adaptive weight tuning law for  $\hat{\mathbf{W}}_a$  is derived as

$$\begin{aligned} \dot{\hat{\mathbf{W}}}_a &= -a_0 [(\mathbf{\Gamma}_a \hat{\mathbf{W}}_a - \mathbf{\Gamma}_b m_{1w} \hat{\mathbf{W}}_c) - \frac{1}{4} \hat{\mathbf{W}}_a \nabla \boldsymbol{\sigma}_w \mathbf{A} \nabla \boldsymbol{\sigma}_w^T \bar{m}_w \\ &\cdot \hat{\mathbf{W}}_c] + \frac{a_0}{2} \Pi(\hat{U}_a) \nabla \boldsymbol{\sigma}_w \mathbf{A} \nabla \Psi, \end{aligned} \quad (72)$$

where  $m_w = \nabla \boldsymbol{\sigma}_w^T (F_V(\mathbf{z}_\Theta) + \mathbf{G}_V \hat{U}_a - X_d)$ ,  $\bar{m}_w = \frac{m_w}{(1+m_w^T m_w)^2}$ ,  $m_{1w} = \frac{m_w}{(1+m_w^T m_w)}$ , and  $\mathbf{A} = \mathbf{G}_V \mathbf{R}_u^{-1} \mathbf{G}_V^T$ .  $c_0 > 0$  and  $a_0 > 0$  are the learning rates of CNN and ANN, respectively.  $\mathbf{\Gamma}_a$  and  $\mathbf{\Gamma}_b$  are tuning matrix and vector to stabilize the system. The expression of  $\Pi(\hat{U}_a)$  is shown as

$$\Pi(\hat{U}_a) = \begin{cases} 0, & \text{if } \nabla \Psi^T (F_V(\mathbf{z}_\Theta) + \mathbf{G}_V \hat{U}_a - X_d) < 0 \\ 1, & \text{otherwise} \end{cases}. \quad (73)$$

The term  $\frac{a_0}{2} \Pi(\hat{U}_a) \nabla \boldsymbol{\sigma}_w \mathbf{A} \nabla \Psi$  is an adaptation term, which ensures the stability of system (53) during the training process and relaxes the requirement of initial stabilizing control. The definition and properties of function  $\Psi$  are given in Assumption 6.

The structure of the nearly optimal control scheme, which is based on the modified ADP approach, is given in Fig. 4.

**Assumption 6.** [49, 50] Suppose that  $\Psi$  is a continuously differentiable radially unbounded Lyapunov function and its gradient along system (53) is  $\nabla \Psi$ . There exists a condition that  $\dot{\Psi} = \nabla \Psi (F_V(\mathbf{z}_\Theta) + \mathbf{G}_V U_a^* - X_d) < 0$  holds. Moreover, we can find a positive-definite matrix  $\mathbf{Q}_\Psi \in \mathbb{R}^{7 \times 7}$  such that  $\dot{\Psi} = -\nabla \Psi \mathbf{Q}_\Psi \nabla \Psi < 0$ .

**Theorem 3.** Consider system (53) with Assumptions 4-6. Design the CNN and ANN as (66) and (67). Then, let the weight

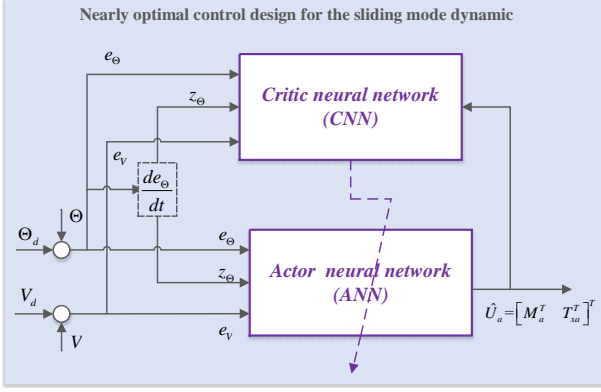


Figure 4: Structure of the nearly optimal control scheme.

tuning laws of two NNs be described by (71) and (72), respectively. Select relative parameters appropriately, then the tracking error vector  $E_V = [e_\Theta, e_V]^T$ , weight estimations errors  $\tilde{W}_c = W_c^* - \hat{W}_c$  and  $\tilde{W}_a = W_a^* - \hat{W}_a$  are UUB.

PROOF. Design the Lyapunov function candidate as follows.

$$V_A = \Psi + V_a^* + L_c + L_a, \quad (74)$$

where  $L_c = \frac{1}{2} \tilde{W}_c^T c_0^{-1} \tilde{W}_c$  and  $L_a = \frac{1}{2} \tilde{W}_a^T a_0^{-1} \tilde{W}_a$ .  $\Psi$  is the continuous Lyapunov function given in Assumption 6. Taking derivative of  $V_A$ , we have

$$\dot{V}_A = \dot{\Psi} + \dot{V}_a^* + \dot{L}_c + \dot{L}_a. \quad (75)$$

First,  $\dot{V}_a^*$  is analyzed. Based on the designed  $\hat{U}_a$ , the derivative of  $V_a^*$  is

$$\begin{aligned} \dot{V}_a^* &= \nabla V_a^* (F_V(z_\Theta) + G_V \hat{U}_a - X_d) \\ &= \delta_{V_A} + A^* F_V(z_\Theta) - A^* X_d \\ &\quad - \frac{1}{2} A^* G_V R_u^{-1} G_V^T A_a, \end{aligned} \quad (76)$$

where  $A^* = 2\beta_w E_V + \nabla \sigma_w^T W_c^*$  and  $A_a = 2\beta_w E_V + \nabla \sigma_w^T \hat{W}_a$ .  $\delta_{V_A} = \nabla \delta_w (F_V(z_\Theta) - \frac{1}{2} G_V R_u^{-1} G_V^T (2\beta_w E_V + \nabla \sigma_w^T \hat{W}_a) - X_d)$ , which satisfies  $\|\delta_{V_A}\| \leq \delta_{V_A1} \|E_V\| + \delta_{V_A2}$ . Noting the fact that

$$\begin{aligned} A^* (F_V(z_\Theta) - X_d) &= -\bar{Q}_E(E_V) + \frac{1}{4} A^* G_V R_u^{-1} G_V^T A^* \\ &\quad + \delta_{HJB} \end{aligned}$$

and  $\bar{Q}_E(E_V) \geq b_E \|E_V\|^2$ . (76) can be transformed into

$$\dot{V}_a^* \leq \delta_{V_A} + \delta_{HJB} - b_E \|E_V\|^2 + \frac{1}{2} A^* G_V R^{-1} G_V^T \tilde{A}_a, \quad (77)$$

where  $\tilde{A}_a = A^* - A_a = \nabla \sigma_w^T \tilde{W}_a$ .

Considering  $\dot{\tilde{W}}_c = -\dot{\hat{W}}_c$ , the derivative of  $L_c$  is

$$\dot{L}_c = \tilde{W}_c^T \frac{m_w}{(1 + m_w^T m_w)^2} [A_c (F_V(z_\Theta) + G_V \hat{U}_a - X_d)$$

$$+ \bar{Q}_E(E_V) + \hat{U}_a^T R_u \hat{U}_a],$$

where  $A_c = 2\beta_w E_V + \nabla \sigma_w^T \hat{W}_c$ . From (65), there exists

$$\begin{aligned} \bar{Q}_E(E_V) &= \delta_{HJB} - A^* (F_V(z_\Theta) - X_d) \\ &\quad + \frac{1}{4} A^{*T} G_V R_u^{-1} G_V^T A^*. \end{aligned} \quad (78)$$

$\dot{L}_c$  is rewritten as

$$\begin{aligned} \dot{L}_c &\leq \tilde{W}_c^T \frac{m_w}{(1 + m_w^T m_w)^2} [-m_w^T \tilde{W}_c + \delta_{HJB} \\ &\quad + \frac{1}{4} \tilde{A}_a G_V R_u^{-1} G_V^T \tilde{A}_a], \end{aligned} \quad (79)$$

where  $\tilde{A}_c = A^* - A_c = \nabla \sigma_w^T \tilde{W}_c$ .

Next, considering  $\dot{\tilde{W}}_a = -\dot{\hat{W}}_a$ , the derivative of  $L_a$  is

$$\begin{aligned} \dot{L}_a &= -\tilde{W}_a^T \Gamma_a \tilde{W}_a + \tilde{W}_a^T \Gamma_a W_c^* - \tilde{W}_a^T \Gamma_b m_{1w} W_c^* \\ &\quad + \tilde{W}_a^T \Gamma_b m_{1w} \tilde{W}_c - \frac{1}{4} \tilde{W}_a^T (W_c^* - \tilde{W}_a) \nabla \sigma_w A \nabla \sigma_w^T \\ &\quad \cdot \bar{m}_w (W_c^* - \tilde{W}_c) - \frac{\tilde{W}_a}{2} \Pi(\hat{U}_a) \nabla \sigma_w A \nabla \Psi. \end{aligned} \quad (80)$$

According to the results in (77), (79), and (80), it is easy to show that

$$\dot{V}_A \leq \bar{\Psi} - X_a^T \Xi_1 X_a + \|\Xi_2\| \|X_a\| + \Xi_3, \quad (81)$$

where  $X_a = [E_V^T, m_{1w} \tilde{W}_c^T, \tilde{W}_a^T]^T$ ,  $\bar{\Psi} = \nabla \Psi^T (F_V(z_\Theta) + G_V \hat{U}_a - X_d) - \frac{\tilde{W}_a}{2} \Pi(\hat{U}_a) \nabla \sigma_w A \nabla \Psi$ .  $\Xi_1$ ,  $\Xi_2$ , and  $\Xi_3$  are shown as follows.

$$\Xi_1 = \begin{bmatrix} \chi_1 & \frac{\chi_5}{2} & \frac{\chi_4}{2} \\ \frac{\chi_5}{2} & \chi_2 & \frac{\chi_6}{2} \\ \frac{\chi_4}{2} & \frac{\chi_6}{2} & \chi_3 \end{bmatrix}, \quad \Xi_2 = [\eta_1, \eta_2, \eta_3]^T,$$

$$\Xi_3 = \delta_{V_A2} + \delta_{HJB}.$$

$$\chi_1 = b_E, \quad \chi_2 = I, \quad \chi_3 = \Gamma_a - \frac{1}{4} \nabla \sigma_w^T A \nabla \sigma_w \bar{m}_w W_c^*$$

$$\chi_4 = -\beta_w A \nabla \sigma_w^T, \quad \chi_5 = 0$$

$$\chi_6 = -\Gamma_b - \frac{\nabla \sigma_w^T A \nabla \sigma_w W_c^* \bar{m}_w}{4}$$

$$\eta_1 = \delta_{V_A1}, \quad \eta_2 = \frac{\delta_{HJB}}{1 + m_w^T m_w},$$

$$\begin{aligned} \eta_3 &= \Gamma_a W_c^* - \Gamma_b m_{1w} W_c^* - \frac{W_c^{*T} \nabla \sigma_w A \nabla \sigma_w^T W_c^* \bar{m}_w}{4} \\ &\quad + \frac{\nabla \sigma_w A \nabla \sigma_w^T W_c^*}{2}. \end{aligned}$$

For matrix  $\Xi_1$ ,  $\Gamma_a$  and  $\Gamma_b$  are selected appropriately to ensure the positive definite of  $\Xi_1$ . Besides, there exist two positive constants  $\delta_{\Xi_2}$  and  $\delta_{\Xi_3}$ , such that  $\|\Xi_2\| \leq \delta_{\Xi_2}$  and  $\|\Xi_3\| \leq \delta_{\Xi_3}$ .

On basis of the result in (80), the following classified discussion is carried out.

*Case 1* ( $\Pi(\hat{U}_a) = 0$ ): In this case, we have

$$\nabla\Psi^T(F_V(\mathbf{z}_\Theta) + \mathbf{G}_V\hat{U}_a - \mathbf{X}_d) < 0.$$

According to [50], there exists a positive constant  $\eta_\Psi$  satisfying  $\nabla\Psi^T(F_V(\mathbf{z}_\Theta) + \mathbf{G}_V\hat{U}_a - \mathbf{X}_d) < -\eta_\Psi \|\nabla\Psi\| < 0$ . (80) is rewritten as

$$\begin{aligned} \dot{V}_A \leq & -\eta_\Psi \|\nabla\Psi\| - \lambda_{\min}(\Xi_1) \left( \|\mathbf{X}_a\| - \frac{\delta_{\Xi_2}}{2\lambda_{\min}(\Xi_1)} \right)^2 \\ & + \frac{\delta_{\Xi_2}^2}{4\lambda_{\min}(\Xi_1)} + \delta_{\Xi_3}. \end{aligned} \quad (82)$$

By (82),  $\dot{V}_A < 0$  when

$$\|\nabla\Psi\| > \frac{\delta_{\Xi_2}^2}{4\eta_\Psi\lambda_{\min}^2(\Xi_1)} + \frac{\delta_{\Xi_3}}{\eta_\Psi} \quad (83)$$

or

$$\|\mathbf{X}_a\| > \frac{\delta_{\Xi_2} + \sqrt{\delta_{\Xi_2}^2 + 4\lambda_{\min}(\Xi_1)\delta_{\Xi_3}}}{2\lambda_{\min}(\Xi_1)}. \quad (84)$$

*Case 2* ( $\Pi(\hat{U}_a) = 1$ ): In this case,  $\tilde{\Psi}$  is transformed into

$$\begin{aligned} \tilde{\Psi} = & \nabla\Psi^T(F_V(\mathbf{z}_\Theta) + \mathbf{G}_V U_a^* - \mathbf{X}_d) - \nabla\Psi^T \mathbf{G}_V \delta_{\text{cou}} \\ \leq & -\eta_x \lambda_{\min}(\mathbf{Q}_\Psi) \|\nabla\Psi\|^2 + \delta_{y1} \|\nabla\Psi\| \end{aligned}$$

with  $\eta_x \in (0, 1)$  and  $\delta_{y1} = \|\mathbf{G}_V\| \bar{\delta}_{\text{cou}}$ . Then, (81) is rewritten as

$$\begin{aligned} \dot{V}_A \leq & -\eta_x \lambda_{\min}(\mathbf{Q}_\Psi) \|\nabla\Psi\|^2 + \delta_{y1} \|\nabla\Psi\| \\ & - \delta_{y0} \|\mathbf{X}_a\|^2 + \delta_{\Xi_2} \|\mathbf{X}_a\| + \delta_{\Xi_3} \\ = & -\eta_x \lambda_{\min}(\mathbf{Q}_\Psi) \left( \|\nabla\Psi\| - \frac{\delta_{y1}}{2\eta_x \lambda_{\min}(\mathbf{Q}_\Psi)} \right)^2 \\ & - \delta_{y0} \left( \|\mathbf{X}_a\| - \frac{\delta_{\Xi_2}}{2\delta_{y0}} \right)^2 + \Xi_4, \end{aligned} \quad (85)$$

where  $\delta_{y0} = \lambda_{\min}(\Xi_1)$  and  $\Xi_4 = \frac{\delta_{\Xi_2}^2}{4\delta_{y0}} + \delta_{\Xi_3} + \frac{\delta_{y1}^2}{4\eta_x \lambda_{\min}(\mathbf{Q}_\Psi)}$ .  $\dot{V}_A$  is negative when

$$\|\nabla\Psi\| > \sqrt{\frac{\Xi_4}{\eta_x \lambda_{\min}(\mathbf{Q}_\Psi)}} + \frac{\delta_{y1}}{2\eta_x \lambda_{\min}(\mathbf{Q}_\Psi)} \quad (86)$$

or

$$\|\mathbf{X}_a\| > \sqrt{\frac{\Xi_4}{\delta_{y0}}} + \frac{\delta_{\Xi_2}}{2\delta_{y0}}. \quad (87)$$

Through the above analysis,  $\nabla\Psi$ ,  $E_V$ ,  $\tilde{\mathbf{W}}_c$ , and  $\tilde{\mathbf{W}}_a$  are UUB. Thus, the tracking error  $\mathbf{e}_\Theta$  and  $e_V$  in attitude and air-speed subsystem are UUB.

The proof of Theorem 3 is completed.

### 3.3. Design procedure of the ADP-ASMC scheme

For system (5) and (7) satisfying Assumption 1-5, the design procedures of the proposed ADP-ASMC scheme is given as follows.

*Step 1:* Utilize the AC structure-based ADP approach to approximately solve the HJB equation (59) of sliding mode dynamics (53). Through (71) and (72), the weight estimation  $\hat{\mathbf{W}}_c$  and  $\hat{\mathbf{W}}_a$  can be obtained. Then, the nearly optimal control laws are given as

$$\begin{bmatrix} \mathbf{M}_a \\ T_{xa} \end{bmatrix} = \hat{U}_a = -\frac{1}{2} \mathbf{R}_u^{-1} \mathbf{G}_V^T (2\beta_w E_V + \nabla\sigma_w^T \hat{\mathbf{W}}_a).$$

*Step 2:* On the basis of the nearly optimal control laws in Step 1, ISMs in two subsystems are formulated as

$$\mathbf{S} = \mathbf{z}_\Theta - \int_0^t \mathbf{R}_\Theta \mathbf{I}^{-1} \mathbf{M}_a - \ddot{\Theta}_d d\tau_t,$$

and

$$S_V = e_V(t) - \int_0^t -g_v - \dot{V}_d + \frac{\cos\alpha \cos\beta T_{xa} - D}{m} d\tau_t.$$

For the above ISMs, the sliding mode control laws are designed as

$$\begin{cases} \mathbf{M}_s = \mathbf{I} \mathbf{R}_\Theta^{-1} (-k_1 \Phi_1(\mathbf{S}) + \mathbf{z}_1 - \mathbf{G}(\mathbf{z}_\Theta)) \\ \dot{\mathbf{z}}_1 = -k_{20} L \Phi_2(\mathbf{S}) \end{cases}$$

with gain-adaptation law (14)-(16), and

$$\begin{cases} T_{xs} = \frac{m}{\cos\alpha \cos\beta} \left( -k_{1v} \sqrt{\frac{L_v}{2}} \phi_{v1} + z_v + \phi_{v3}(L_v, \phi_{v1}) \right) \\ \dot{z}_v = -k_{2v} L_v \phi_{v2} \end{cases}$$

with gain-adaptation law (40)-(41), respectively.

*Step 3:* Following Step 1 and Step 2, set the control laws for fixed-wing UAV as

$$\begin{bmatrix} \mathbf{M} \\ T_x \end{bmatrix} = \begin{bmatrix} \mathbf{M}_s \\ T_{xs} \end{bmatrix} + \begin{bmatrix} \mathbf{M}_a \\ T_{xa} \end{bmatrix}.$$

To illustrate the overall control architecture clearly in our work, the schematic diagram of the proposed ADP-ASMC scheme is shown in Fig. 5

## 4. NUMERICAL SIMULATIONS

In this section, numerical simulations are conducted for demonstrating the efficiency of the proposed ADP-ASMC scheme. The simulation scenarios, results, and analysis are all given.

The parameters of fixed-wing UAV used in our work refer to [30] and [44]. The initial conditions of fixed-wing UAV are:  $\Theta_0 = [5.8, -11.5, 11.5]^T$  (deg),  $\omega_0 = [0.58, 1.15, 1.72]^T$  (deg/s), and  $V_0 = 0.4$  (m/s). The nominal inertia matrix  $\mathbf{I}$  is:  $I_{xx} = 0.5528$ ,  $I_{yy} = 0.6335$ ,  $I_{zz} = 1.0783$ , and  $I_{xz} = 0.0015$ . The matched disturbance  $\Delta \mathbf{d}_m$ , unmatched

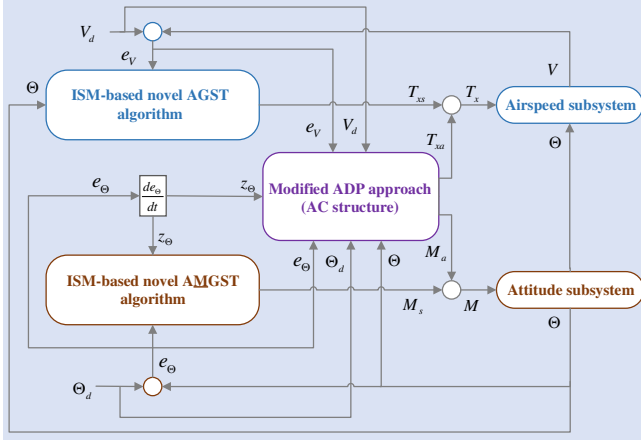


Figure 5: Schematic diagram of ADP-ASMC scheme.

disturbance  $\Delta d_u$ , and external disturbance  $\Delta V(t)$  are given as follows.

$$\Delta d_m = \begin{cases} [0; 0; 0]^T, & 0 < t < 5 \\ [1.5 \sin(\pi t/17); 0.8 \sin(\pi t/15); 1.1 \sin(\pi t/16)]^T, & \end{cases}$$

$$\Delta d_u = [2.1 \sin(\pi t/19); 2.1 \sin(\pi t/19); 2.1 \sin(\pi t/19)],$$

$$\Delta V = \begin{cases} 0, & 0 < t < 6 \\ 5 \sin(0.2t), & t \geq 6 \end{cases}$$

The numerical simulations are implemented on MATLAB/SIMULINK environment and the integration step is specified as 1ms.

In this part, the proposed attitude control scheme is compared with two control methods, i.e., the linear sliding surface-based adaptive second order sliding mode (LSS-ASOSM) in [30] and adaptive continuous twisting algorithm (ACTA) in [51]. The LSS-ASOSM is designed on the basis of linear sliding surface and adaptive second order sliding mode. In addition, the designed airspeed control scheme is contrasted with ASOSM in [30] and fast terminal sliding mode surface-based generalized super-twisting (FTSM-GST) method. It should be noted that the FTSM-GST method is derived from [52]. The FTSM surface is given as

$$S_{vf} = e_v + k_s \int_0^t [e_v]^{\gamma_{f1}} + [e_v]^{\gamma_{f2}} d\tau$$

with  $k_s > 0$ ,  $\gamma_{f1} \geq 1$ , and  $\gamma_{f2} \in (0, 1)$ . The thrust based on FTSM-GST method is given as

$$T_x = \frac{m}{\cos \alpha \cos \beta} \left[ \frac{D}{m} + g_v + \dot{V}_d - ks([e_v]^{\gamma_{f1}} + [e_v]^{\gamma_{f2}}) - k_{1f} \phi_{f1} + z_f \right]$$

$$\dot{z}_f = -k_{2f} \phi_{f2}, \quad (88)$$

where  $\phi_{f1} = [S_{vf}]^{\frac{1}{2}} + S_{vf}$  and  $\phi_{f2} = \frac{1}{2}[S_{vf}]^0 + \frac{3}{2}[S_{vf}]^{\frac{1}{2}} + S_{vf}$ .

The parameter setting of the ISM-based AMGST controller (for attitude subsystem) and ISM-based AGST controller (for airspeed subsystem) are given in Table 1.

Table 1

The parameters of ISM-based AMGST and ISM-based AGST.

Controller	Parameters
ISM-based AMGST	$\kappa_1 = 8, \kappa_0 = 0.2,$ $L_0 = 0.3, al = 0.99,$ $\epsilon = 0.01, \lambda_0 = 0.01, \bar{r} = 10,$ $\bar{e} = 0.1, r_m = 0.6.$
	$k_{1v} = 5, k_{2v} = 3, L_{v0} = 0.55,$ $l_v = 0.99, \lambda_{v0} = 0.01, \epsilon_v = 0.05$ $e_b = 0.3, \bar{r}_v = 5, r_{mv} = 0.5.$

Table 2

The parameters of LSS-ASOSM, ACTA, ASOSM and FTSM-GST.

Controller	Parameters
LSS-ASOSM	$\lambda_l = 1, k = 15,$ $\mu = 0.005, K_{\min} = 0.8,$ $c = 1.35.$
	$l = 5, k_{1r} = 1.1; k_{2r} = 1.1,$ $k_{3r} = 1.2, k_{4r} = 1.2.$
ASOSM	$k_V = 12, \mu = 0.01,$ $K_{V\min} = 0.8, \epsilon_V = 1.$
FTSM-GST	$\gamma_{f1} = 1.2, \gamma_{f2} = 0.88, k_s = 1.5,$ $k_{1f} = 4, k_{2f} = 1.5.$

The control parameters of nearly optimal controller are provided as follows. The matrices  $Q_E$  and  $R_u$  are set as:  $Q_E = 1.5 \times I_7$  and  $R_u = \text{diag} \{1.2, 1.23, 1, 2.2\}$ . The initial weight values in CNN and ANN are selected in the range  $(0, 2]$  randomly. The number of neurons in CNN and ANN is  $N = 35$  and the activation function vector is selected as

$$\sigma_w(\hat{E}_V) = [e_{\theta 1}^2, e_{\theta 1} e_{\theta 2}, e_{\theta 2}^2, e_{\theta 1} e_{\theta 3}, e_{\theta 3}^2, e_{\theta 2} e_{\theta 3}, z_{\theta 1}^2, z_{\theta 1} z_{\theta 2}, z_{\theta 2}^2, z_{\theta 1} z_{\theta 3}, z_{\theta 3}^2, z_{\theta 2} z_{\theta 3}, e_{\theta 1}^3 z_{\theta 1}, e_{\theta 2}^3 z_{\theta 2}, e_{\theta 3}^3 z_{\theta 3}, e_{\theta 1} z_{\theta 1} z_{\theta 2}, e_{\theta 2} z_{\theta 2} z_{\theta 3}, e_{\theta 3} z_{\theta 3} z_{\theta 1}, e_{\theta 1} z_{\theta 2}, e_{\theta 1} z_{\theta 3}, e_{\theta 2} z_{\theta 1}, e_{\theta 2} z_{\theta 3}, e_{\theta 3} z_{\theta 1}, e_{\theta 3} z_{\theta 2}, z_{\theta 1}^3 e_{\theta 3} e_{\theta 2}, z_{\theta 2}^3 e_{\theta 1} e_{\theta 3}, z_{\theta 3}^3 e_{\theta 1} e_{\theta 2}, e_{\theta 1} z_{\theta 1}^3, e_{\theta 2} z_{\theta 2}^3, e_{\theta 3} z_{\theta 3}^3, e_v^2, e_v e_{\theta 1}, e_v e_{\theta 2}, e_v e_{\theta 3}^3, e_v e_{\theta 2}^3]^T.$$

In Table 2, the control parameters of the ACTA, ASOSM, LSS-ASOSM, and FTSM-GST are specified. The specific definition of parameters in four comparative control methods can refer to [30], [51], and [52].

The tracking performance under ACTA, LSS-ASOSM, and ADP-ASMC are shown in Figs. 6 and 7. The attitude angles  $\phi$ ,  $\theta$ , and  $\psi$  can track the reference command under the three control methods. From the local figures in Fig. 7, the ADP-ASMC performs better than the other two control methods when the unmatched disturbance  $\Delta d_u$  is imposed at  $t = 5s$ .

In Fig. 8, tracking errors  $e_\phi, e_\theta, e_\psi$  are presented. Fig. 9 shows the control moments  $M_x, M_y, M_z$ . From Fig. 8,

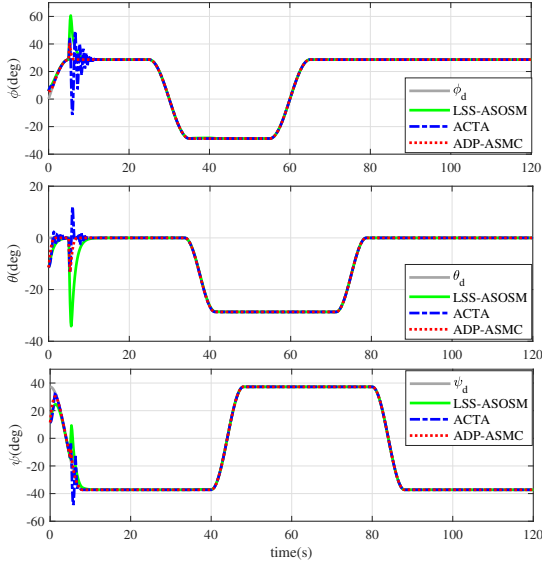


**Figure 6:** Tracking performance of attitude subsystem under LSS-ASOSM, ACTA, and ADP-ASMC in 0-120s.

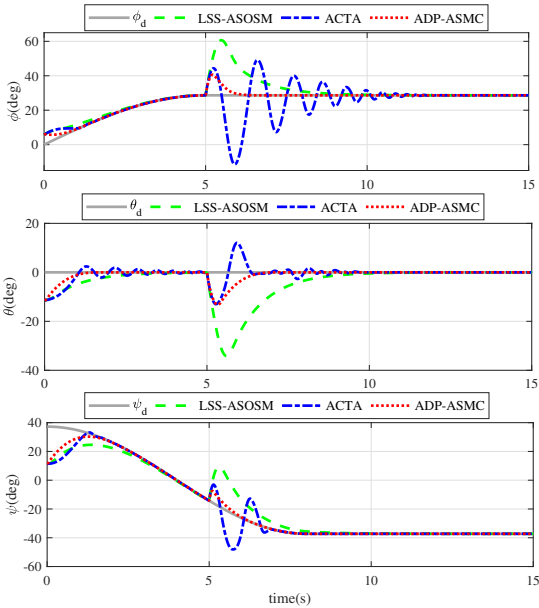


**Figure 7:** Tracking performance of attitude subsystem under LSS-ASOSM, ACTA, and ADP-ASMC in 0-15s.

we can see that the tracking errors can be stabilized through three control methods. From the simulation results in Fig. 9, the chattering amplitude in ADP-ASMC are much smaller than that of the other two control methods, which is beneficial for the actuators. The reason lies in two aspects: i). The modified gain-adaptation laws (14)-(16) help avoid the overestimation of control gains. ii). The modified ADP approach can generate nearly optimal control moments  $\mathbf{M}_a$ , which optimizes the energy consumption to some extent. The performance index comparisons among three control

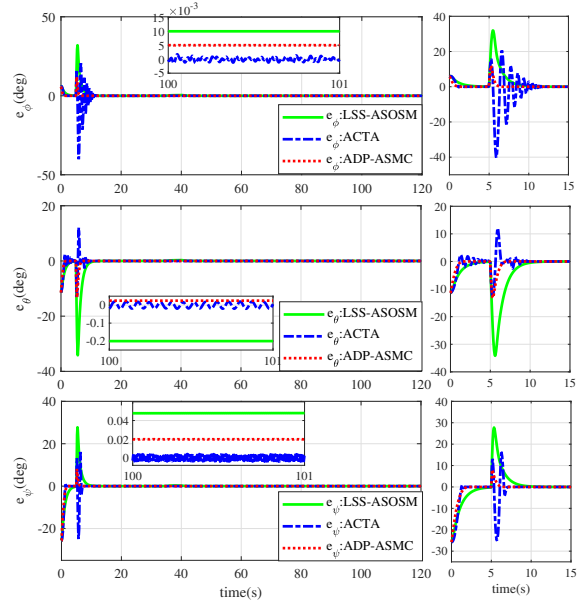


**Figure 8:** Tracking errors of  $\phi$ ,  $\theta$ ,  $\psi$  under LSS-ASOSM, ACTA, and ADP-ASMC.

methods presented in Fig. 10 has also illustrated above point. The integral absolute error (IAE)  $\int_0^{120} (|e_\phi| + |e_\theta| + |e_\psi|) dt$  and integral absolute control moment (IACM)  $\int_0^{120} (|M_x| + |M_y| + |M_z|) dt$  are used as performance indexes. It is obvious that the proposed ADP-ASMC outperforms the existing LSS-ASOSM and ACTA. ADP-ASMC achieves the satisfactory tracking performance and the least energy consumption.

Fig. 11 shows the control gains. We can observe that the control gain  $L_a$  in ACTA is monotonically increasing and is much larger than that in LSS-ASOSM and ADP-ASMC. Then, control moments with aggressive chattering are generated (shown in Fig. 9). In proposed ADP-ASMC, the control gain  $k_{20}L$  changes with the disturbance. From Fig. 11, although the control gains  $K_{1\theta}$  and  $K_{2\theta}$  are smaller than  $k_1$  and  $k_{20}L$ , respectively, the convergence precision of tracking errors under LSS-ASOSM is lower than that under the other two control methods.

The variations of the attitude angular rates including  $p$ ,  $q$ , and  $r$  under three methods are shown in Fig. 12. It is found that the angular rates of ADP-ASMC change with smaller chattering and faster convergence compared with the other two control methods.

The tracking performance of the airspeed subsystem under ASOSM, FTSM-GST and ADP-ASMC are presented in Fig. 13. The airspeed  $V$  can track the reference command  $V_d$  under three control methods. In comparison with the other two control methods, the proposed ADP-ASMC achieves smaller overshoot. Moreover, the thrust  $T_x$  and tracking error  $e_V$  are depicted in Fig. 14. In the top sub-graph of Fig. 14, the thrust  $T_x$  generated by ADP-ASMC is smaller than that of the other two control methods. Besides, similar to the attitude subsystem,  $\int_0^{120} |e_V| dt$  and  $\int_0^{120} T_x dt$

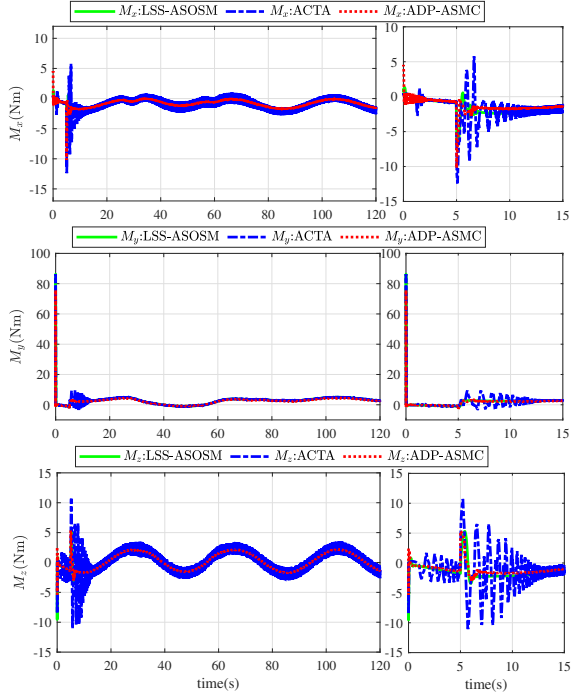


**Figure 9:** Control moments  $M_x$ ,  $M_y$ ,  $M_z$  of LSS-ASOSM, ACTA, and ADP-ASMC.

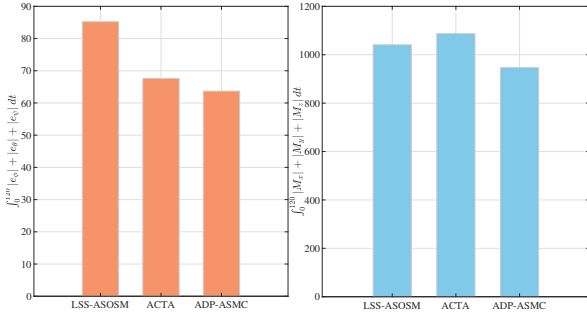
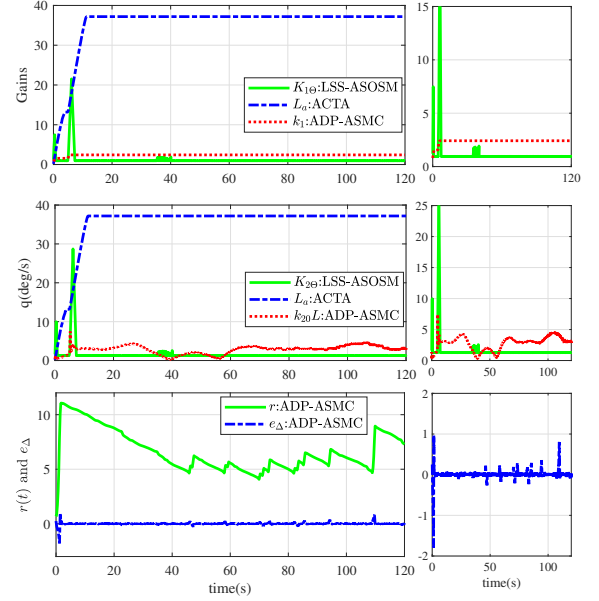


**Figure 10:** Performance index of three control schemes.

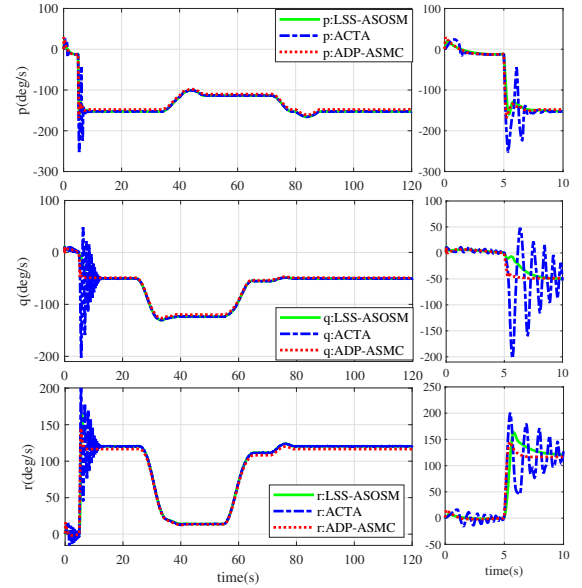
are selected as performance indexes to evaluate the control performances of three control methods in airspeed subsystem. The performance index comparisons among FTSM-GST, ASOSM, and ADP-ASMC are shown in Fig. 15. Through the simulation results in Figs. 13-15, it is explicit that the proposed ADP-ASMC achieves better dynamic characteristics and lower energy consumption.

Fig. 16 shows the control gains in three control methods. After  $t = 6s$ , the control gains in ASOSM and ADP-ASMC are smaller than that in FTSM-GST. However, the convergence precision of ASOSM is lower than that of the other two methods (see the local curves of  $e_V$  in Fig. 14). In the bottom sub-graph of Fig. 16,  $r_v$  and  $\bar{e}_v$  are also presented.  $\bar{e}_v$  is limited in a finite domain and  $r_v$  starts decreasing after 9s.

Fig. 17 depicts the evolution of CNN and ANN weight



**Figure 11:** Control gains of LSS-ASOSM, ACTA, and ADP-ASMC.



**Figure 12:** Angular rates  $p$ ,  $q$ ,  $r$  of LSS-ASOSM, ACTA, and ADP-ASMC.

vectors  $\hat{W}_c$  and  $\hat{W}_a$ . As indicated in Fig. 17, the weights are dramatically adapting during the early stage and the weight vectors of CNN and ANN are both convergent after a few seconds.

## 5. Conclusion

In our work, the adaptive dynamic programming-based adaptive-gain sliding mode control (ADP-ASMC) scheme is proposed for fixed-wing UAV subject to unknown distur-

Title:

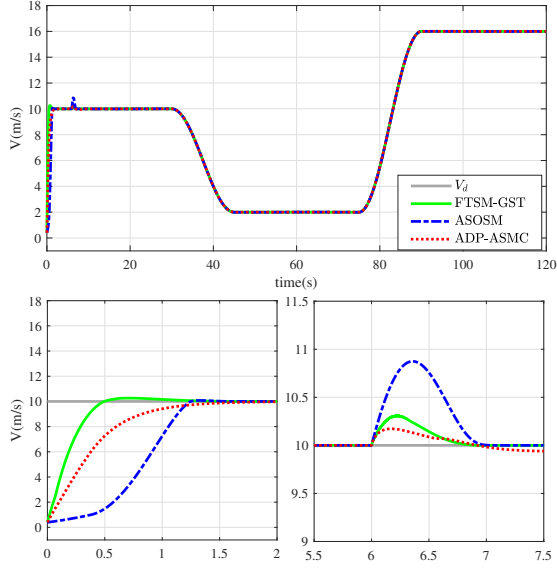


Figure 13: Tracking performance of airspeed subsystem under FTSM-GST, ASOSM, and ADP-ASMC.

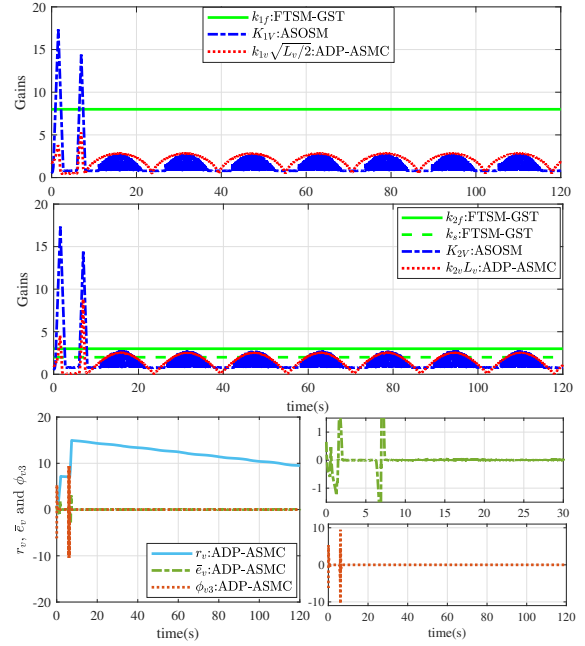


Figure 16: Control gains of FTSM-GST, ASOSM and ADP-ASMC.

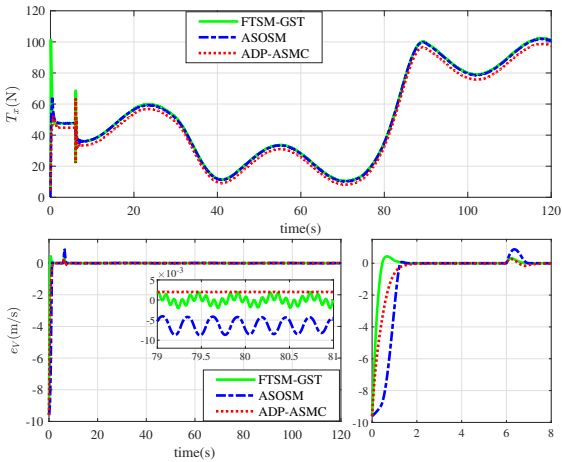


Figure 14: Thrust  $T_x$  and tracking error  $e_V$ .

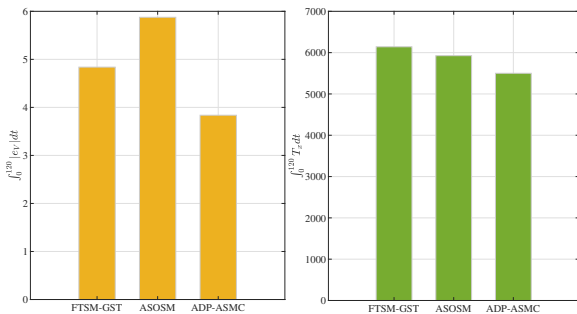


Figure 15: Performance index comparisons of three control schemes.

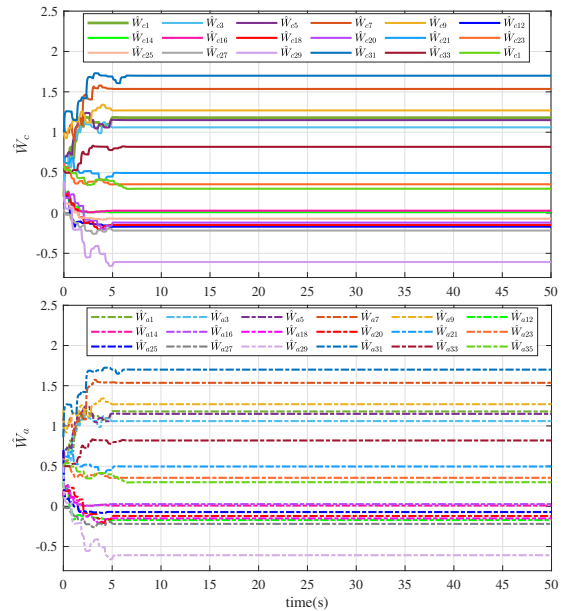


Figure 17: Weight estimations  $\hat{W}_c$  and  $\hat{W}_a$  of CNN and ANN.

bances. Aiming at the different issues in two subsystems, the ISM-based AMGST and ISM-based AGST, which are designed via two novel AGST algorithms, are utilized to reject the unknown disturbances such that the equivalent sliding-mode dynamics can be obtained. Unlike the existing adaptive-gain sliding mode algorithms, the two gains in the novel AMGST are tuned through two different gain-adaptation laws so as to address the state- and time-dependent disturbance



better and attenuate chattering efficiently. Then, a modified ADP approach is constructed to generate the nearly optimal control laws for the sliding-mode dynamics. In this approach, the requirement of initial stabilizing control is relaxed. Compared with the conventional sliding mode controllers, the proposed ADP-ASMC scheme provides stronger robustness and meanwhile reduces the energy consumption of fixed-wing UAV. Simulation results show that the ADP-ASMC scheme can provide better control performance and demonstrates the superiority of the proposed control scheme.

## References

- Wang, N., Ahn, C.K.. Coordinated trajectory tracking control of a marine aerial-surface heterogeneous system. *IEEE/ASME Trans Mechatron* 2021;doi:10.1109/TMECH.2021.3055450.
- Ren, Y., Chen, M.. Anti-swing control for a suspension cable system of a helicopter with cable swing constraint and unknown dead-zone. *Neurocomputing* 2019;356:257–267.
- Kang, Y., Hedrick, J.K.. Linear tracking for a fixed-wing UAV using nonlinear model predictive control. *IEEE Trans Control Syst Technol* 2009;17(5):1202–1210. doi:10.1109/TCST.2008.2004878.
- Dou, R., Duan, H.. Pigeon inspired optimization approach to model prediction control for unmanned air vehicles. *Aircr Eng Aerosp Tec* 2016;88(1):108–116. doi:10.1108/AEAT-05-2014-0073.
- Shao, X., Liu, J., Cao, H., Shen, C., Wang, H.. Robust dynamic surface trajectory tracking control for a quadrotor UAV via extended state observer. *Int J Robust Nonlin Control* 2018;28(7):2700–2719. doi:10.1002/rnc.4044.
- Böhm, E., Coates, E.M., Moe, S., Johansen, T.A.. Deep reinforcement learning attitude control of fixed-wing UAVs using proximal policy optimization. In: *Proc. IEEE Int. Conf. Unmanned Aircr. Syst. (ICUAS)*. 2019:523–533. doi:10.1109/ICUAS.2019.8798254.
- Smith, J., Su, J., Liu, C., Chen, W.. Disturbance observer based control with anti-windup applied to a small fixed wing UAV for disturbance rejection. *J Intell Robot Syst* 2017;88:329–346. doi:10.1007/s10846-017-0534-5.
- Li, P., Yu, X., Peng, X., Zheng, Z., Zhang, Y.. Fault-tolerant cooperative control for multiple UAVs based on sliding mode techniques. *Sci China Inf Sci* 2017;60:070204. doi:10.1007/s11432-016-9074-8.
- Cao, L., Ren, H., Meng, W., Li, H., Lu, R.. Distributed event triggering control for six-rotor UAVs with asymmetric time-varying output constraints. *Sci China Inf Sci* 2020;doi:10.1007/s11432-020-3128-2.
- Li, P., Ma, J., Zheng, Z.. Disturbance-observer-based fixed-time secondorder sliding mode control of an air-breathing hypersonic vehicle with actuator faults. *Proc Inst Mech Eng, Part G: J Aerosp Eng* 2018;232(2):344–361. doi:10.1177/0954410016683732.
- Yu, X., Li, P., Y, Z.. The design of fixed-time observer and finite-time fault-tolerant control for hypersonic gliding vehicles. *IEEE Trans Ind Electron* 2017;65(5):4135–4144. doi:10.1109/TIE.2017.2772192.
- Muñoz, F., González-Hernández, I., Salazar, S., Espinoza, E.S., Lozano, R.. Second order sliding mode controllers for altitude control of a quadrotor uas: Real-time implementation in outdoor environments. *Neurocomputing* 2017;233:61–71.
- Ding, S., Park, J.H., Chen, C.C.. Second-order sliding mode controller design with output constraint. *Automatica* 2020;112:108704. doi:10.1016/j.automatica.2019.108704.
- Qi, W., Gao, X., Ahn, C.K., Cao, J., Chen, J.. Fuzzy integral sliding-mode control for nonlinear Semi-Markovian switching systems with sppllication. *IEEE Trans Syst, Man, Cybern, Syst* 2020;doi:10.1109/TSMC.2020.3034484.
- Chen, F., Jiang, R., Zhang, K., Jiang, B., Tao, G.. Robust backstepping sliding-mode control and observer-based fault estimation for a quadrotor UAV. *IEEE Trans Ind Electron* 2016;63(8):5044–5056. doi:10.1109/TIE.2016.2552151.
- Mofid, O., Mobayen, S.. Adaptive sliding mode control for finite-time stability of quad-rotor UAVs with parametric uncertainties. *ISA transactions* 2018;72:1–4. doi:10.1016/j.isatra.2017.11.010.
- Delavari, H., Mohadeszadeh, M.. Robust finite-time synchronization of non-identical fractional-order hyperchaotic systems and its application in secure communication. *IEEE/CAA Journal of Automatica Sinica* 2016;6(1):228–235.
- Plestan, F., Shtessel, Y., Brégeault, V., A, P.. New methodologies for adaptive sliding mode control. *Int J control* 2010;83(9):1097–1919. doi:10.1080/00207179.2010.501385.
- Lee, H., Utkin, V.I.. Chattering suppression methods in sliding mode control systems. *Annu Rev Control* 2007;31(2):179–188. doi:10.1016/j.arcontrol.2007.08.001.
- Li, P., Yu, X., Xiao, B.. Adaptive quasi-optimal higher order sliding-mode control without gain overestimation. *IEEE Trans Ind Inf* 2017;14(9):3881–3891. doi:10.1109/TII.2017.2787701.
- Shtessel, Y., Taleb, M., Plestan, F.. A novel adaptive-gain super twisting sliding mode controller: Methodology and application. *Automatica* 2012;48(5):759–769. doi:10.1016/j.automatica.2012.02.024.
- Shtessel, Y.B., Moreno, J.A., Plestan, F., Fridman, L.M., Poznyak, A.S.. Super-twisting adaptive sliding mode control: A Lyapunov design. In: *Proc. 49th IEEE Int. Conf. Decision and Control (CDC)*. 2010:5109–5113. doi:10.1109/CDC.2011.6160982.
- Edwards, C., Shtessel, Y.B.. Adaptive continuous higher order sliding mode control. *Automatica* 2016;65:183–190. doi:10.1016/j.automatica.2015.11.038.
- Edwards, C., Shtessel, Y.B.. Adaptive dual-layer supertwisting control and observation. *Int J Control* 2016;89(9):1759–1766. doi:10.1080/00207179.2016.1175030.
- Obeid, H., Laghrouche, S., Fridman, L., Chitour, Y., Harmouche, M.. Barrier function-based variable gain super-twisting controller. *IEEE Trans Autom Control* 2020;65(11):428–4933. doi:10.1109/TAC.2020.2974390.
- Zhang, C., Zhang, G., Dong, Q.. Fixed-time disturbance observer-based nearly optimal control for reusable launch vehicle with input constraints. *ISA transactions* 2021;.
- Dong, Q., Zong, Q., Tian, B., Wang, F.. Adaptive-gain multivariable super-twisting sliding mode control for reentry RLV with torque perturbation. *Int J Robust Nonlinear Control* 2017;27(4):620–638. doi:10.1002/rnc.3589.
- Guo, Z., Chang, J., Guo, J., Zhou, J.. Adaptive twisting sliding mode algorithm for hypersonic reentry vehicle attitude control based on finite-time observer. *ISA transactions* 2018;77:20–29. doi:10.1016/j.isatra.2018.04.001.
- Wu, X., Xiao, B., Qu, Y.. Modeling and sliding modebased attitude tracking control of a quadrotor UAV with time-varying mass. *ISA Transactions* 2019;doi:10.1016/j.isatra.2019.08.017.
- Castañeda, H., Salas-Peña, O.S., de León-Morales, J.. Extended observer based on adaptive second order sliding mode control for a fixed wing UAV. *ISA transactions* 2017;66:226–232. doi:10.1016/j.isatra.2016.09.013.
- Zhang, C., Zhang, G., Dong, Q.. Multi-variable finite-time observer-based adaptive-gain sliding mode control for fixed-wing uav. *IET Control Theory & Applications* 2021;15(2):223–247.
- Laghrouche, S., Harmouche, M., Chitour, Y., Obeid, H., Fridman, L.M.. Barrier function-based adaptive higher order sliding mode controllers. *Automatica* 2021;123:109355.
- Yang, X., He, H.. Adaptive dynamic programming for decentralized stabilization of uncertain nonlinear large-scale systems with mismatched interconnections. *IEEE Trans Syst, Man, Cybern, Syst* 2020;50(8):2870–2882. doi:10.1109/TSMC.2018.2837899.
- Wen, G., Chen, C.L.P., Ge, S.S., Yang, H., Liu, X.. Optimized adaptive nonlinear tracking control using actor-critic reinforcement learning strategy. *IEEE Trans Ind Inf* 2019;15(9):4969–4977. doi:10.1109/TII.2019.2894282.
- Yang, X., He, H., Zhong, X.. Approximate dynamic programming for nonlinear-constrained optimizations. *IEEE Trans Cybern* ????(in press). doi:10.1109/TCYB.2019.2926248.

36. Yang, X., He, H., Zhong, X.. Adaptive dynamic programming for robust regulation and its application to power systems. *IEEE Trans Ind Electron* 2018;65(7):5722–5732. doi:10.1109/TIE.2017.2782205.
37. Zhong, X., He, H.. An event-triggered ADP control approach for continuous-time system with unknown internal states. *IEEE Trans Cybern* 2016;47(3):683–694. doi:10.1109/TCYB.2016.2523878.
38. Mu, C., Ni, Z., Sun, C., He, H.. Air-breathing hypersonic vehicle tracking control based on adaptive dynamic programming. *IEEE Trans Neural Netw Learn Syst* 2017;28(3):584–598. doi:10.1109/TNNLS.2016.2516948.
39. Tang, Y., Mu, C., He, H.. Near-space aerospace vehicles attitude control based on adaptive dynamic programming and sliding mode control. In: *Proc. 2017 IEEE Int. Joint Conf. Neural Networks (IJCNN)*. 2017;doi:10.1109/IJCNN.2017.7966009.
40. Fan, Q.Y., Yang, G.H.. Adaptive actor-critic designbased integral slidingmode control for partially unknown nonlinear systems with input disturbances. *IEEE Trans Neural Netw Learn Syst* 2016;27(1):165–177. doi:10.1109/TNNLS.2015.2472974.
41. Zhang, H., Park, J.H., Yue, D., Zhao, W.. Nearly optimal integral sliding-mode consensus control for multiagent systems with disturbances. *IEEE Trans Syst, Man, Cybern, Syst* 2019;doi:10.1109/TSMC.2019.2944259.
42. Zhang, H., Qu, Q., Xiao, G., Cui, Y.. Optimal guaranteed cost sliding mode control for constrained-input nonlinear systems with matched and unmatched disturbances. *IEEE Trans Neural Netw Learn Syst* 2018;29(6):2112–2126. doi:10.1109/TNNLS.2018.2791419.
43. Xia, R., Chen, M., Wu, Q., Wang, Y.. Neural network based integral sliding mode optimal flight control of near space hypersonic vehicle. *Neurocomputing* 2020;379:41–52. doi:10.1016/j.neucom.2019.10.038.
44. Stevens, B.L., Lewis, F.L., Johnson, E.N.. Aircraft control and simulation: Dynamics, controls design, and autonomous systems. John Wiley and Sons; 2015. doi:10.1002/9781119174882.
45. Filippov, A.F.. Differential equations with discontinuous righthand sides: Control systems. Springer Science and Business Media; 2013.
46. Utkin, V.I., Poznyak, A.S.. Adaptive sliding mode control with application to super-twist algorithm: Equivalent control method. *Automatica* 2013;49:39–47. doi:10.1016/j.automatica.2012.09.008.
47. Castillo, I., Fridman, L., Moreno, J.A.. Super-twisting algorithm in presence of time and state dependent perturbations. *Int J Control* 2018;91(11):2535–2548. doi:10.1080/00207179.2016.1269952.
48. Bhat, S.P., Bernstein, D.S.. Finite-time stability of continuous autonomous systems. *SIAM J Control Optim* 2000;38(3):751–766. doi:10.1137/S0363012997321358.
49. Guo, X., Yan, W., Cui, R.. Reinforcement learning-based nearly optimal control for constrained-input partially unknown systems using differentiator. *IEEE Trans Neural Netw Learn Syst* 2020;31(11):4713–4725. doi:10.1109/TNNLS.2019.2957287.
50. Liu, D., Wei, Q., Wang, D., Yang, X., Li, H.. Adaptive dynamic programming with applications in optimal control. Berlin: Springer International Publishing; 2017. doi:10.1007/978-3-319-50815-3.
51. Moreno, J.A., Negrete, D.Y., Torres-González, V., Fridman, L.. Adaptive continuous twisting algorithm. *Int J Control* 2016;89(9):1798–1806. doi:10.1080/00207179.2015.1116713.
52. Dong, Q., Zong, Q., Tian, B., Wang, F.. Integrated finite-time disturbance observer and controller design for reusable launch vehicle in reentry phase. *J Aerosp Eng* 2017;30(1):04016076. doi:10.1061/(ASCE)AS.1943-5525.0000670.